nature metabolism

ARTICLES

https://doi.org/10.1038/s42255-020-0228-3

Eosinophils regulate adipose tissue inflammation and sustain physical and immunological fitness in old age

Daniel Brigger[1,2], Carsten Riether[3,4], Robin van Brummelen[1,2], Kira I. Mosher[5,13], Alicia Shiu[5,14], Zhaoqing Ding[5,15], Noemi Zbären[1,2], Pascal Gasser[1,2], Pascal Guntern[1,2], Hanadie Yousef[5], Joseph M. Castellano[6], Federico Storni[1,2,16], Neill Graff-Radford[7], Markus Britschgi[5,17], Denis Grandgirard[8], Magdalena Hinterbrandner[3,4], Mark Siegrist[2], Norman Moullan[9], Willy Hofstetter[2], Stephen L. Leib[8], Peter M. Villiger[1,2], Johan Auwerx[9], Saul A. Villeda[10], Tony Wyss-Coray[5,11], Mario Noti[12,18,19] ✉ and Alexander Eggel[1,2,19] ✉

Adipose tissue eosinophils (ATEs) are important in the control of obesity-associated inflammation and metabolic disease. However, the way in which ageing impacts the regulatory role of ATEs remains unknown. Here, we show that ATEs undergo major age-related changes in distribution and function associated with impaired adipose tissue homeostasis and systemic low-grade inflammation in both humans and mice. We find that exposure to a young systemic environment partially restores ATE distribution in aged parabionts and reduces adipose tissue inflammation. Approaches to restore ATE distribution using adoptive transfer of eosinophils from young mice into aged recipients proved sufficient to dampen age-related local and systemic low-grade inflammation. Importantly, restoration of a youthful systemic milieu by means of eosinophil transfers resulted in systemic rejuvenation of the aged host, manifesting in improved physical and immune fitness that was partially mediated by eosinophil-derived IL-4. Together, these findings support a critical function of adipose tissue as a source of pro-ageing factors and uncover a new role of eosinophils in promoting healthy ageing by sustaining adipose tissue homeostasis.

White adipose tissue (WAT), besides its established role in nutrient sensing and energy storage, is a highly active endocrine organ that undergoes significant changes in distribution and function with progression of age[1]. Emerging studies suggest that the development of frailty and age-related morbidities is accelerated by the loss of WAT homeostasis, while strategies that delay or limit WAT dysfunction have been shown to enhance health and lifespan across species[2–12]. WAT is home to a dense network of immune cells including lymphocytes, group-2 innate lymphoid cells, macrophages and eosinophils, which have the capacity to regulate tissue homeostasis and metabolism[13]. While eosinophils are well known for their cytotoxic effector functions in allergic responses and host protection against parasitic infections[14], recent studies have emphasized the importance of adipose tissue eosinophils (ATEs) in the maintenance of alternatively activated adipose tissue macrophages (ATMs) and the control of obesity-associated WAT inflammation in metabolic disease[15,16]. While obesity and ageing share numerous biological similarities related to WAT dysfunction[17], it remains to be determined whether ATEs can regulate WAT homeostasis and organismal health in old age. Here, we identify WAT as a major source of the pro-ageing factor CCL11 (ref. [18]), a potent chemoattractant for eosinophils that accumulates systemically with age and negatively correlates with ATE distribution in humans and mice. These age-related changes were closely associated with WAT dysfunction and systemic low-grade inflammation, two significant risk factors for both morbidity and mortality in the elderly[1,19,20]. We find that eosinophils from young organisms preferentially migrate to WAT of aged mice, restore WAT function and dampen systemic low-grade inflammation, in a manner partially mediated by eosinophil-derived IL-4. Importantly, restoration of a

[1]Department of Rheumatology, Immunology and Allergology, Bern University Hospital, University of Bern, Bern, Switzerland. [2]Department for BioMedical Research, University of Bern, Bern, Switzerland. [3]Tumor Immunology, Department for BioMedical Reserach, University of Bern, Bern, Switzerland. [4]Department of Medical Oncology, Inselspital, Bern University Hospital, University of Bern, Bern, Switzerland. [5]Department of Neurology and Neurological Sciences, Stanford University School of Medicine, Stanford, CA, USA. [6]Nash Family Department of Neuroscience, Department of Neurology, Friedman Brain Institute, Ronald M. Loeb Center for Alzheimer's Disease, Icahn School of Medicine at Mount Sinai, New York, NY, USA. [7]Department of Neuroscience, Mayo Clinic, Jacksonville, FL, USA. [8]Institute for Infectious Diseases, University of Bern, Bern, Switzerland. [9]Laboratory of Integrative and Systems Physiology, École Polytechnique Fédérale de Lausanne, Lausanne, Switzerland. [10]Department of Anatomy, University of California San Francisco, San Francisco, CA, USA. [11]Wu Tsai Neurosciences Institute, Stanford University, Stanford, CA, USA. [12]Institute of Pathology, Division of Experimental Pathology, University of Bern, Bern, Switzerland. [13]Present address: Department of Chemical and Biological Engineering, University of California, Berkeley, CA, USA. [14]Present address: Amplitude Analytics Inc., San Francisco, CA, USA. [15]Present address: Johnson & Johnson Pharmaceutical Research & Development, L.L.C., San Diego, CA, USA. [16]Present address: Department for Visceral Surgery and Medicine, Bern University Hospital, University of Bern, Bern, Switzerland. [17]Present address: Roche Pharma Research and Early Development, Neuroscience Discovery, Roche Innovation Center Basel, F. Hoffmann-La Roche Ltd, Basel, Switzerland. [18]Present address: Department of Gastrointestinal Health, Immunology, Nestlé Research, Lausanne, Switzerland. [19]These authors contributed equally: Mario Noti, Alexander Eggel. ✉e-mail: mario.noti@rd.nestle.com; alexander.eggel@dbmr.unibe.ch

youthful environment by means of eosinophil transfers translated into systemic rejuvenation of the aged host, supporting a previously unrecognized role of eosinophils in promoting healthy ageing.

Results

Age-related changes in the systemic environment partially originate in WAT. To identify soluble blood factors that accumulate with age, we employed a proteomic approach to measure 170 hormones, cytokines, chemokines and other secreted signalling proteins in plasma of ageing humans and mice (Supplementary Tables 1 and 2). Analysis of the 67 and 51 detectable factors (Supplementary Table 3) in human and mouse plasma, respectively, revealed a clear blood-based systemic ageing signature (Fig. 1a,b). Unsupervised clustering of normalized mean protein levels separated sample groups according to age in both species. Furthermore, we identified nine plasma proteins among a total of 41 overlapping factors that significantly correlate with age in humans and mice (Fig. 1c and Supplementary Table 4). In agreement with the results of previous studies[18], we find that CCL11 (Eotaxin-1) and CCL2 (MCP-1) rank amongst the top age-correlating factors (Supplementary Table 5) in plasma of both humans (Fig. 1d,e) and mice (Fig. 1f,g), with an absence of sex-specific differences. To determine the biological origin of increased systemic CCL11 and CCL2 levels, we performed tissue screens in aged mice. Among 12 tissues assessed and in line with previous reports[21], WAT represents a major source of CCL11 and CCL2 (Extended Data Fig. 1a–d), which significantly increase with age (Extended Data Fig. 1e,f).

Age-related WAT inflammation is associated with altered adipose tissue eosinophil distribution. Given that the pro-ageing factor CCL11 is a potent chemoattractant for eosinophils, we next assessed eosinophil distribution in visceral WAT. Using histological and flow cytometric approaches, we identified the presence of ATEs in both humans (Fig. 2a–e, Extended Data Fig. 2a and Supplementary Table 6) and mice (Fig. 2g,h and Extended Data Fig. 2d). Despite the observed age-related increase of CCL11 levels in WAT, we find an inverse correlation with ATE frequencies (Fig. 2e,i) while absolute numbers remain unchanged (Extended Data Fig. 2e). In contrast, but consistent with an age-related increase in WAT CCL2 levels, both frequencies and numbers of ATMs increase with age (Fig. 2i and Extended Data Fig. 2e), resulting in a significantly lower ATE/ATM ratio in WAT of aged compared to young mice. Reduced ATE frequencies in aged humans and mice were further associated with visceral adipose tissue inflammation, apparent by a significant increase in *Il6* and *Il1β* (Fig. 2f,j) and adipocyte hypertrophy (Extended Data Fig. 2b,c,f,g). These data suggest that age-related changes in systemic CCL11 and CCL2 levels and associated alterations in ATE distribution are conserved in both humans and mice, and may contribute to WAT dysfunction in old age.

Exposure to a young systemic environment restores ATE/ATM ratios and limits WAT inflammation. Given the rejuvenating potential of a youthful environment on muscle, bone, heart, brain and central nervous system[22–27], we next assessed whether exposure of aged mice to a young circulation has the potential to restore WAT homeostasis. To do so, we took advantage of heterochronic parabiosis[28], a model system in which two animals of different age are joined to share a common circulatory system (Fig. 3a). In line with reduced ATE and increased ATM frequencies in aged mice (Fig. 2i), we observed similar changes in old isochronic parabionts (Fig. 3b,c). Strikingly, exposure to a young systemic milieu resulted in partial restoration of ATE/ATM ratios in WAT of old heterochronic parabionts compared to old isochronic controls (Fig. 3b,c). To assess whether changes in ATE/ATM ratios are due to homing of young eosinophils into old WAT, we paired young green fluorescent protein (GFP)-reporter mice to either young or aged wild-type mice through parabiosis (Fig. 3e) and assessed the frequency of GFP-positive eosinophils in WAT. Employing this model system we found GFP-positive eosinophils in WAT of old heterochronic wild-type mice, indicating that eosinophils from young parabionts efficiently migrate into WAT of their aged partners (Fig. 3f,g). We further observed similar percentages of GFP-negative eosinophils in the WAT of young isochronic and heterochronic GFP-reporter mice (Fig. 3f,g), implying that eosinophils from the old parabiont retain their migratory capacity when exposed to a young systemic environment. Given the reported immunoregulatory properties of eosinophils in WAT[15,29,30], we next assessed whether restoration of ATE/ATM ratios in old heterochronic mice was associated with alterations in adipose tissue inflammation. Strikingly, expression levels of *Il6*, *Ccl2* and *Il1b* in WAT of old heterochronic parabionts were significantly reduced compared to those in old isochronic mice (Fig. 3d). Collectively, these data indicate that age-related changes in ATE/ATM ratios and associated WAT inflammation can be partially restored by exposure to a youthful systemic environment.

Transferred eosinophils predominantly home to WAT and reduce local and systemic inflammation. To assess whether restoration of ATEs is sufficient to resolve ageing signatures in WAT, we transferred eosinophils from young mice into aged recipients. Owing to the limiting numbers of eosinophils in wild-type mice, we used sort-purified eosinophils from IL-5 transgenic mice (C57BL/6J-Tg (Il5)1638Jlee)[31] for adoptive transfers. In a first approach, we adoptively transferred sort purified IL-5 transgenic GFP$^+$ eosinophils to aged recipients to assess the tissue distribution and surface marker phenotype of transferred cells (Fig. 4a and Extended Data Fig. 3a,b). Among 11 tissues assessed, we find that transferred eosinophils predominantly home to WAT of aged mice (Fig. 4a,b) with no alterations in Siglec-F surface expression compared to WAT resident endogenous eosinophils (Extended Data Fig. 3c–e). Given the preferential homing of transferred eosinophils to WAT, we next assessed whether a prolonged protocol of eosinophil transfers to aged mice has functional consequences for age-related WAT dysfunction. To do so, aged mice were injected twice weekly for 4 consecutive weeks with either PBS control (Aged-PBS), eosinophils (Aged-yEOS) or control granulocytes (Aged-yNEU) from young donors (Fig. 4c and Extended Data Fig. 4a). Flow cytometric analyses confirmed preferential homing of transferred eosinophils to WAT, resulting in the restoration of ATE/ATM ratios in aged recipients (Fig. 4d), while no changes in ATE/ATM ratios in mice transferred with control granulocytes were observed (Extended Data Fig. 4b). Consistent with observed changes in ATE/ATM ratios and the reduction of WAT inflammation in old heterochronic parabionts, the levels of pro-inflammatory mediators IL-6, CCL2 and IL-1β were significantly reduced in WAT of Aged-yEOS compared to Aged-PBS mice (Fig. 4e). Additionally, Aged-yEOS mice showed a significant reduction in age-related adipose tissue hypertrophy (Extended Data Fig. 2f,g) indicating that transferred eosinophils have the capacity to control age-related WAT dysfunction. No such changes in response to eosinophil transfers were observed in subcutaneous adipose tissue (Extended Data Fig. 5a–e), nor did transfer of a control granulocyte population affect age-related WAT parameters (Extended Data Fig. 4c). Furthermore, reduced WAT inflammation in Aged-yEOS mice correlated with decreased systemic plasma levels of IL-6, CCL2 and IL-1β (Fig. 4f), supporting the hypothesis that ageing visceral WAT may represent an important source of pro-inflammatory mediators that fuel systemic low-grade inflammation and ageing phenotypes.

Many of the immunoregulatory properties of ATEs have been attributed to their production of IL-4 (ref. [15]). To assess whether the observed reduction in local and systemic low-grade inflammation in response to eosinophil transfers is regulated through eosinophil-derived IL-4, we transferred IL-4-deficient eosinophils derived from IL-5 transgenic young mice into aged recipients

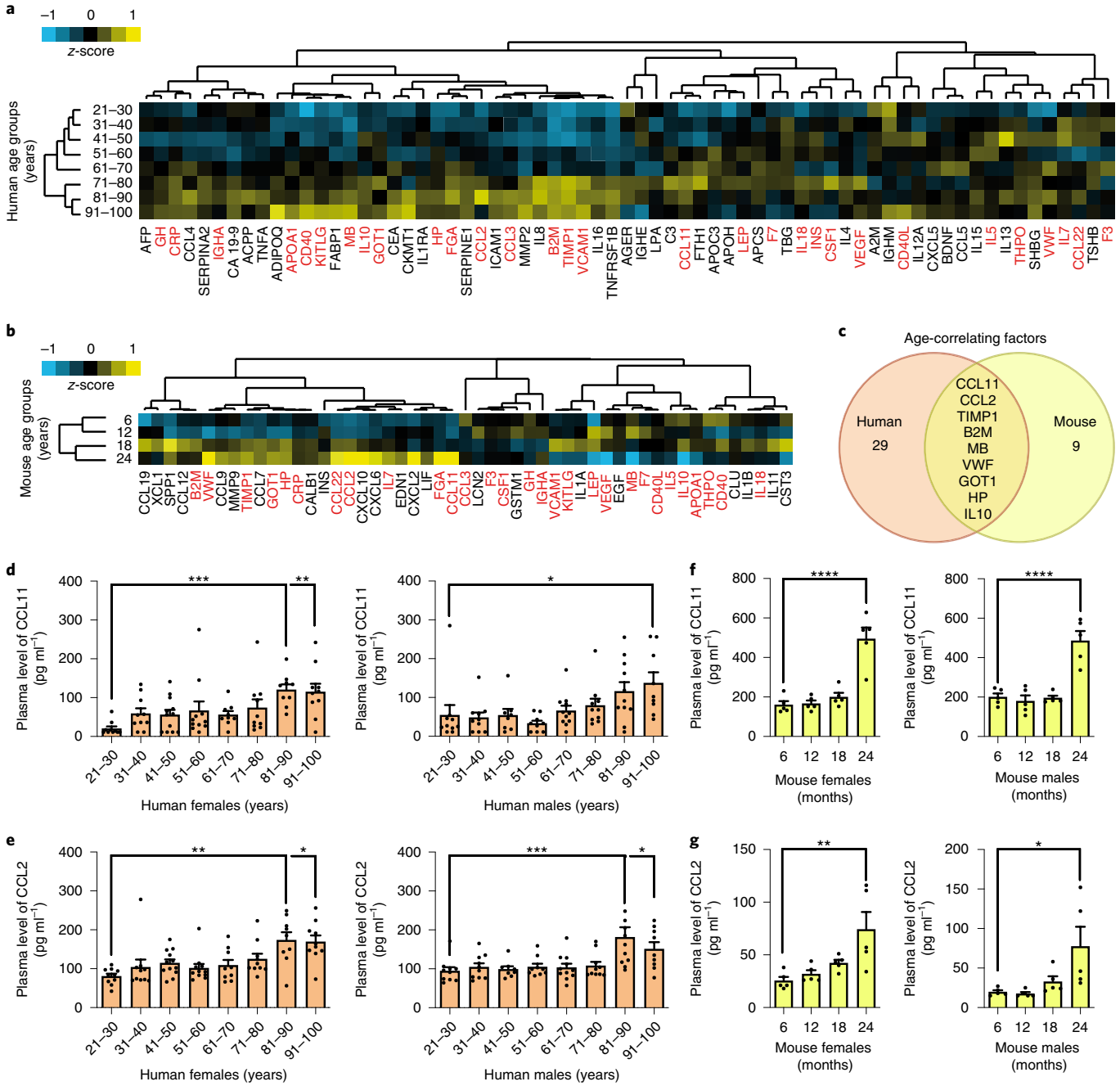

Fig. 1 | Age-related changes in the plasma proteome of humans and mice. a,**b**, Unsupervised clustering of different age groups (humans, $n=20$ per group; mice, $n=10$ per group) based on the levels of 67 human plasma factors (**a**) and 40 mouse plasma factors (**b**). Means of *z*-scored values were used for clustering, and are indicated by colour code ranging from blue (negative) to yellow (positive). Each factor is denominated with its official Human Genome Organization gene nomenclature. Red labels indicate factors that were detectable in both human and mouse cohorts. (**c**) Venn diagram representing plasma factors significantly correlating with age in humans ($n=160$ biologically independent donors) and mice ($n=40$). **d**,**e**, Sex-specific protein levels of CCL11 (**d**) and CCL2 (**e**) in human plasma ($n=10$ per group). **f**,**g**, Plasma levels of CCL11 (**f**) and CCL2 (**g**) in male and female mice ($n=5$ per group) of indicated age groups. Correlations between plasma factor level and age were calculated using Pearson's *r*. Statistical significance was calculated by one-way ANOVA followed by two-tailed post hoc Dunnett's multiple comparison against the youngest group. Wherever possible, data are shown as individual data points with mean ± s.e.m. * $P<0.05$, ** $P<0.01$, *** $P<0.001$, **** $P<0.0001$.

(Aged-yEOS$^{IL4-/-}$). Transfer of both IL-4-sufficient and -deficient eosinophils restored ATE/ATM ratios (Fig. 4d), with eosinophil-derived IL-4 being sufficient to reduce local and systemic age-related increases in IL-6, CCL2 and IL-1β when compared to Aged-PBS controls (Fig. 4e,f). While ATEs have been reported to control obesity-associated WAT inflammation and metabolic disease, their restoration in aged mice by means of adoptive eosinophil transfer from young donors did not alter glucose metabolism (Extended Data Fig. 6a,b). Together, these data indicate that transfer of eosinophils from young donors reduces age-related WAT dysfunction and systemic low-grade inflammation in aged recipients, a mechanism that is in part regulated via eosinophil-intrinsic IL-4.

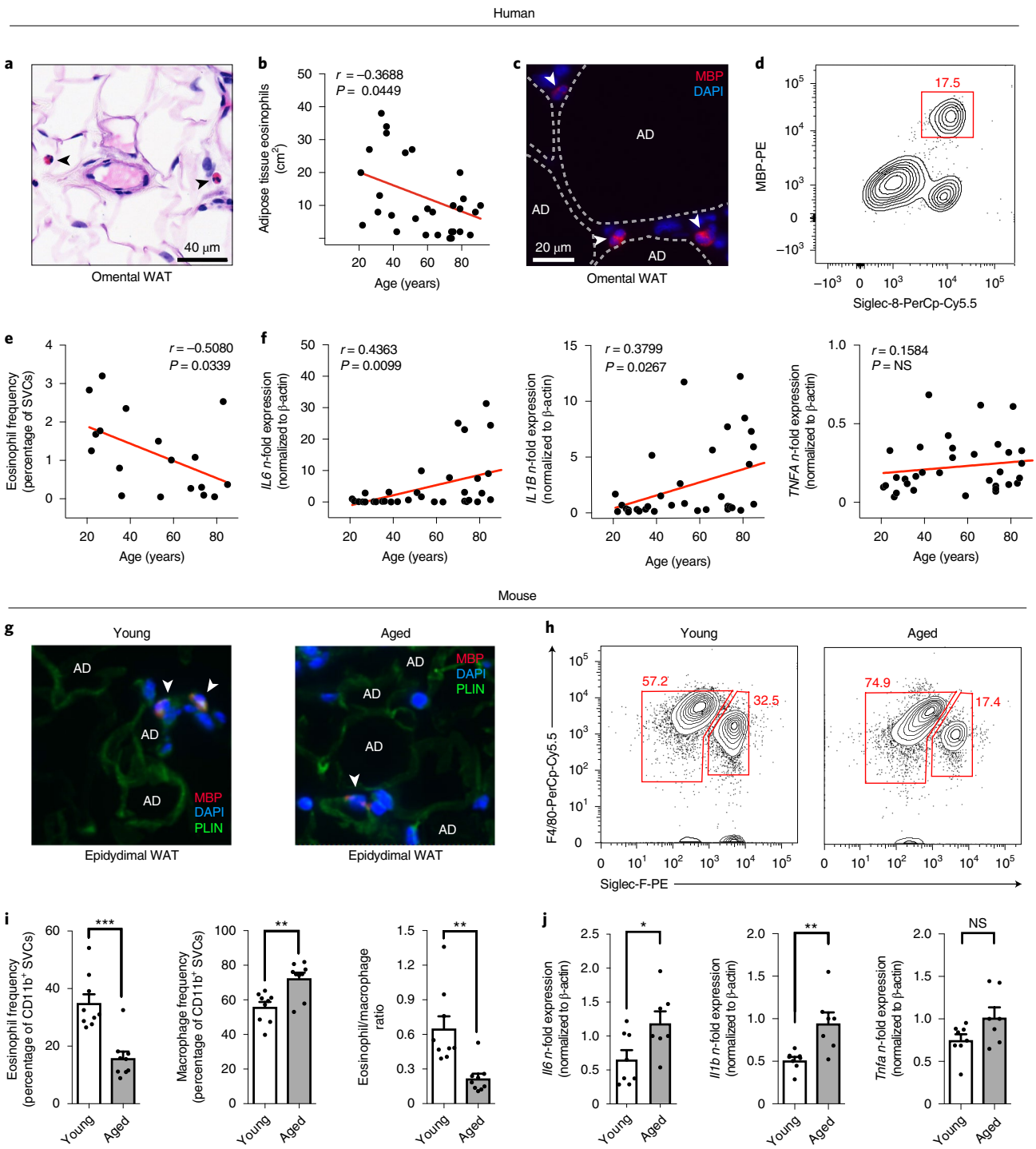

Fig. 2 | Age-related changes in innate immune cell distribution of WAT in humans and mice. a, Representative image of H&E-stained human omental adipose tissue. Arrowheads indicate eosinophils **b**, Quantification of tissue-resident eosinophils in H&E-stained sections of human omental adipose tissue ($n = 30$ biologically independent human donors). **c**, Representative images of MBP-stained human omental adipose tissue. Arrowheads indicate MBP-positive eosinophils. AD, adipocytes. One out of three independently performed experiments is shown. **d**,**e**, Representative flow plots of MBP- and Siglec-8-positive eosinophils (**d**) and corresponding quantification of eosinophil frequencies (**e**) in the SVC fraction of human omental adipose tissue ($n = 18$ biologically independent human donors). **f**, Fold induction of *Tnfa*, *Il1β* and *Il6* messenger RNA expression levels in human omental adipose tissue ($n = 34$ biologically independent human donors). **g**, Representative images of MBP-stained mouse epididymal WAT. Arrowheads indicate MBP-positive eosinophils. Adipocytes are stained for perilipin (PLIN). One out of three independently performed experiments is shown. **h**, Representative flow plots of adipose tissue macrophage ATM (F4/80$^+$, Siglec-F$^-$) and ATE (F4/80^{int}, Siglec-F$^+$) populations in eWAT from young (3 months) and aged (20 months) mice. **i**, Frequencies of eosinophils and macrophages, and calculated eosinophil/macrophage ratio, in eWAT of young and aged mice ($n = 9$ per group). **j**, Fold induction of *Tnfa*, *Il1β* and *Il6* mRNA expression levels in eWAT of young ($n = 8$) and aged mice ($n = 7$). Data are presented as fold expression over aged mice and were pooled from two independently performed experiments. Statistical significance was calculated by unpaired two-tailed Student's *t*-test (**i**,**j**), Pearson's correlation coefficient between eosinophils and age (**b**,**e**) or by fold gene expression levels and age (**f**). Results are shown as individual data points with mean ± s.e.m. * $P < 0.05$, ** $P < 0.01$, *** $P < 0.001$. NS, not significant.

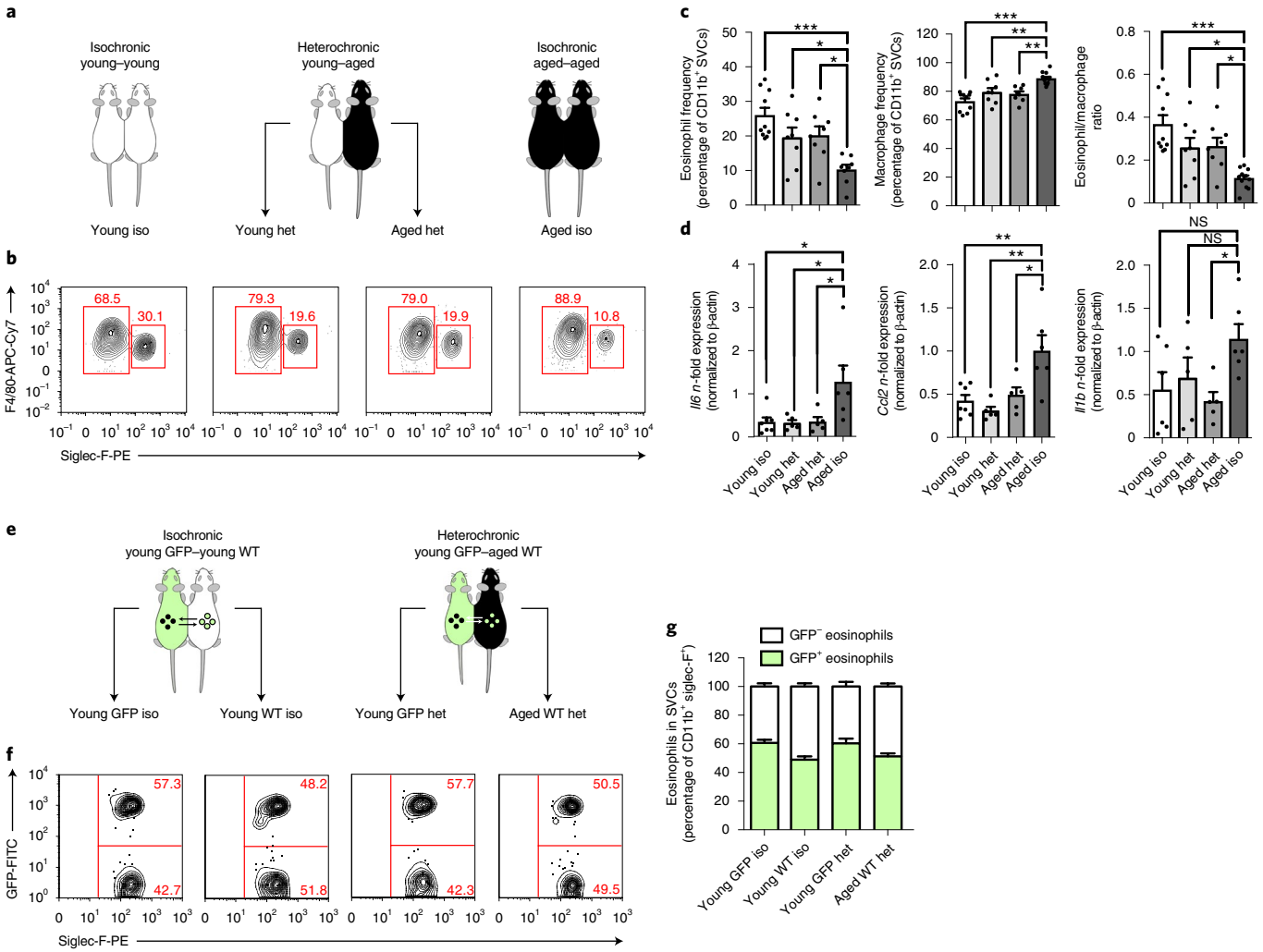

Fig. 3 | Heterochronic parabiosis restores ATE/ATM ratios and limits WAT inflammation. a, Experimental protocol. **b**, Representative flow plots of ATE (F4/80^{int}, Siglec-F^{+}) and ATM (F4/80^{+}, Siglec-F^{-}) populations in eWAT of iso- (Iso) and heterochronic (Het) parabionts. **c**, Frequencies of ATEs and ATMs and calculated ATE/ATM ratios from two independently performed and pooled experiments in eWAT of parabiosed mice (young isochronic, $n=10$; young heterochronic, $n=8$; old heterochronic, $n=8$; old isochronic, $n=12$). **d**, mRNA expression levels for *Il6*, *Ccl2* (young isochronic, $n=7$; young heterochronic, $n=5$; old heterochronic, $n=5$; old isochronic, $n=6$) and *Il1β* (young isochronic, $n=6$; young heterochronic, $n=5$; old heterochronic, $n=5$; old isochronic, $n=6$) in eWAT of parabiosed mice. Data are presented as fold expression over old isochronic controls and are pooled from two independently performed experiments. **e**, Experimental protocol. Isochronic and heterochronic parabiosis was performed by joining young (2–3 months) GFP-reporter mice (GFP) to either young (2–3 months) or aged (18 months) wild-type (WT) C57BL/6 mice. **f**, Representative flow plots of GFP^{+} and GFP^{-} eosinophils in WAT of isochronic or heterochronic parabionts. **g**, Percentages of GFP^{+} and GFP^{-} eosinophils in WAT of young GFP iso ($n=5$), Young GFP het ($n=5$), young WT iso ($n=5$) and aged WT het mice ($n=5$). The experiment was performed once. Statistical significance was calculated by one-way ANOVA followed by two-tailed post hoc Dunnett's multiple comparison test against the aged isochronic group (**c**,**d**). Wherever possible, data are shown as individual data points with mean ± s.e.m. * $P<0.05$, ** $P<0.01$, *** $P<0.001$. NS, not significant.

Eosinophils from young donors improve physical fitness in aged hosts. The activity pattern of ageing organisms continuously decreases as they become sedentary, with widespread consequences for WAT distribution and function[32]. To assess whether improved WAT homeostasis and the associated decrease in systemic inflammation in Aged-yEOS mice translates into improved physical fitness, we performed voluntary and forced physical exercise tests. No changes in voluntary activity were apparent among the different groups (Extended Data Fig. 7a,b). While we observed a significant age-related loss of forced physical performance between Young and Aged-PBS treated mice (Fig. 5a,b,e,f), comparison of pre- to post-transfer measurements in maximal force (grip strength) and endurance tests (RotaRod) revealed significant intra-individual improvements in Aged-yEos mice but not in Aged-PBS controls or Aged-yEOS$^{IL4-/-}$ littermates (Fig. 5c,g). Furthermore, intergroup comparison showed significant physical improvements in both tests exclusively in Aged-yEOS mice, highlighting a rejuvenating potential of IL-4-competent eosinophils in aged hosts (Fig. 5d,h). No alterations in either voluntary or forced physical tests were observed in aged mice transferred with a control granulocyte population (Aged-yNEU) (Extended Data Figs. 4d and 7). The fact that Aged-yEOS mice showed increased physical fitness over aged-PBS controls suggests that transfer of eosinophils to aged hosts may have a direct effect on muscle function. To test this hypothesis, we quantified muscle stem cells (satellite cells) from the hindlimb, which have been reported to progressively decrease with age[33]. Although eosinophil transfers into aged mice partially restored an age-related decrease in muscle stem cells, no changes in muscle mass, fibre size,

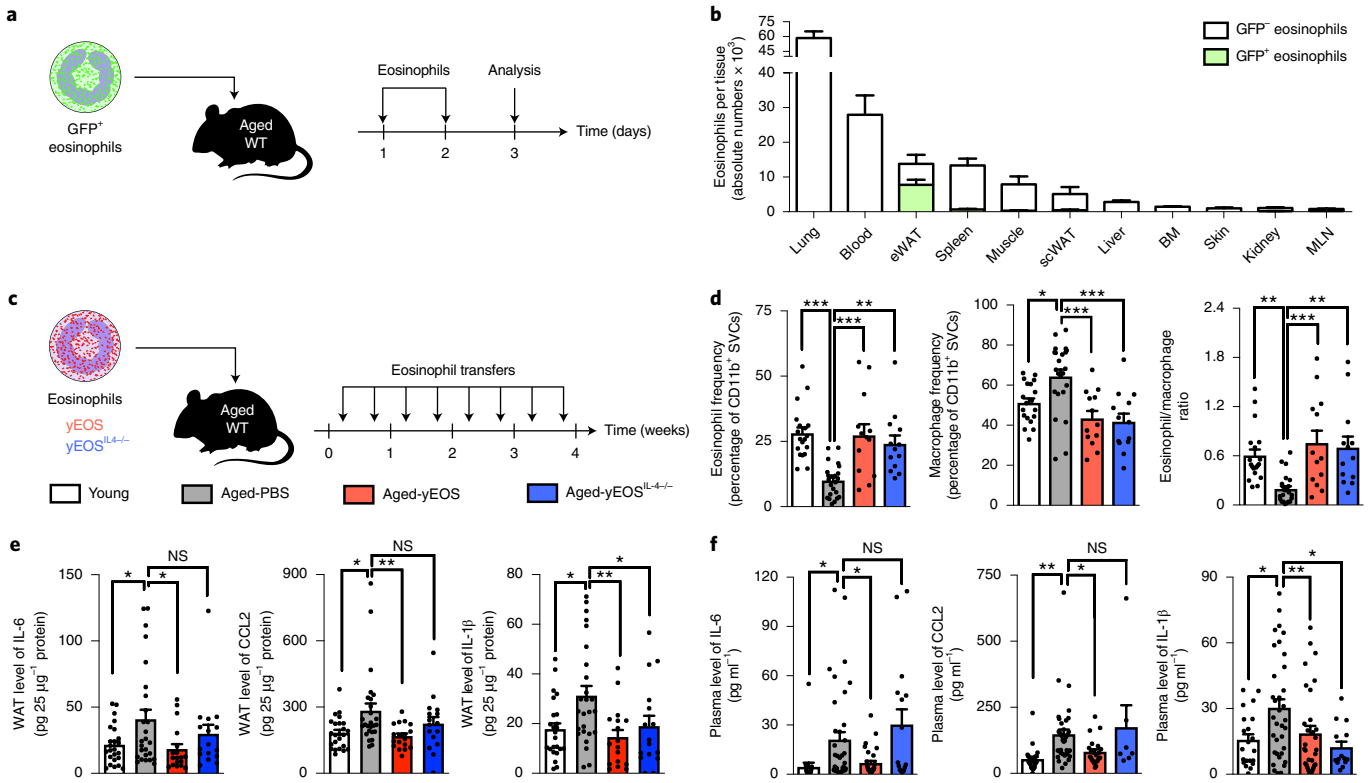

Fig. 4 | Transfer of eosinophils from young donors reverses ageing signatures in WAT and limits systemic inflammation. a,**b**, Aged mice (18 months) were adoptively transferred with sort-purified GFP$^+$ eosinophils on two subsequent days. The following day, eosinophil recruitment into different tissues was assessed by flow cytometry. **a**, Experimental protocol. **b**, Number of GFP$^+$ and GFP$^-$ resident eosinophils in indicated tissues. Data are representative of $n=4$ per group. One of two independently performed experiments is shown. **c**, Experimental protocol. **d**, Frequencies of ATEs and ATMs and calculated ATE/ATM ratios in eWAT of Young ($n=19$), Aged-PBS ($n=23$), Aged-yEOS ($n=13$) and Aged-yEOS$^{IL\text{-}4\text{-}/\text{-}}$ ($n=13$) mice. **e**, Protein levels in eWAT of Young ($n=24$), Aged-PBS ($n=26$), Aged-yEOS ($n=18$) and Aged-yEOS$^{IL\text{-}4\text{-}/\text{-}}$ ($n=16$) mice. **f**, Plasma protein levels of IL-6 and IL-1β in Young ($n=20$), Aged-PBS ($n=35$), Aged-yEOS ($n=32$) and Aged-yEOS$^{IL\text{-}4\text{-}/\text{-}}$ ($n=14$) mice, and CCL2 plasma protein levels of Young ($n=26$), Aged-PBS ($n=37$), Aged-yEOS ($n=22$) and Aged-yEOS$^{IL\text{-}4\text{-}/\text{-}}$ ($n=7$) mice. Statistical significance was calculated by one-way ANOVA followed by two-tailed post hoc Dunnett's multiple comparison test against the Aged-PBS group (**d**–**f**) and, wherever possible, results are shown as individual data points with mean ± s.e.m. * $P<0.05$, ** $P<0.01$, *** $P<0.001$. NS, not significant.

number of centrally nucleated myofibres and ex vivo myogenic potential of muscle stem cells were measured (Extended Data Fig. 8a–g). In addition to the low number of transferred eosinophils in muscle tissue (Fig. 4b), these data indicate that improvement in physical fitness observed in Aged-yEOS mice is most likely to be mediated through indirect effects.

Despite the fact that eosinophils do not carry the IL-5 transgene, alterations in gene expression profiles of eosinophil progenitors derived from transgenic and wild-type mice have been reported[34]. To assess whether eosinophils from wild-type mice might have similar rejuvenating effects on aged mice, we generated bone marrow (BM)-derived eosinophils (BMDEs) from young wild-type mice for subsequent adoptive transfer experiments (Extended Data Fig. 4h). Consistent with results obtained using eosinophils derived from IL-5 transgenic mice, wild-type BDMEs were sufficient to restore ATE/ATM ratios, dampen WAT and systemic IL-6 concentrations and improve physical fitness in aged mice (Extended Data Fig. 4i–m). Together these data indicate that eosinophils derived from both IL-5 transgenic mice and wild-type donors have the potential to improve age-related deterioration in physical fitness.

Homing of adoptively transferred eosinophils to WAT is required to improve physical fitness in aged hosts. Next, we assessed whether homing of adoptively transferred eosinophils to WAT of aged mice is required for the observed reversal of ageing signatures. Previous studies reported the efficacy of pertussis toxin (PT) in inhibition of the migration of eosinophils from BM to peripheral tissues[35]. Adopting a similar approach, sort-purified and CSFE-labelled IL-5 transgenic eosinophils were pretreated ex vivo with a concentration of PT not affecting survival before transfer into aged mice (Aged-yEOS^{PT}) (Fig. 6a). This treatment regimen significantly inhibited eosinophil homing to WAT (Fig. 6b). Consistent with impaired homing to WAT, repetitive transfer of PT-pretreated eosinophils to aged mice failed to recapitulate the beneficial effects on WAT inflammation and physical fitness of vehicle-treated eosinophils (Fig. 6c–h). Together, these data indicate that eosinophils have the potential to improve age-related deterioration of physical fitness by reducing WAT inflammation, a process that is mediated through homing of transferred eosinophils to WAT.

Systemic IL-6 neutralization partially mimics the phenotype of eosinophil-induced amelioration of physical fitness. Our data suggest that reducing systemic low-grade inflammation by means of eosinophil transfer to aged hosts is sufficient to reverse age-related declines in physical fitness. To further test this hypothesis, we targeted systemic IL-6 in aged mice by means of blocking antibodies, one of the key cytokines associated with inflamm-ageing that was significantly reduced following eosinophil transfer into aged mice. To do so, aged mice were injected with an IL-6-blocking antibody

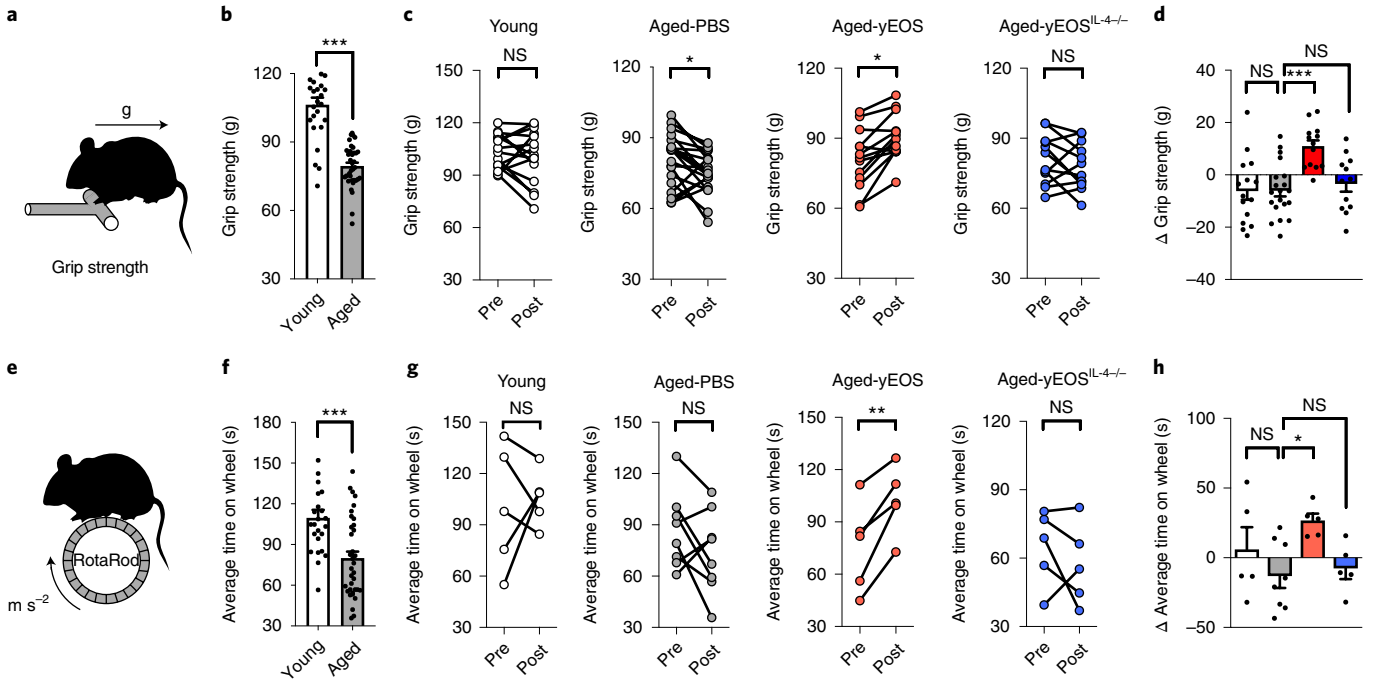

Fig. 5 | Eosinophils from young donors improve physical fitness in aged hosts. a, Schematic grip strength test. **b**, Age-related changes in physical performance in young (3 months, $n=24$) and aged mice (20 months, $n=35$). **c**,**d**, Intra- (**c**) and intergroup (**d**) comparisons of maximal force (grip strength) of Young ($n=15$), Aged-PBS ($n=18$), Aged-yEOS ($n=13$) and Aged-yEOS$^{IL-4-/-}$ ($n=12$) mice. Pooled data from two independently performed experiments are shown. **e**, Schematic of RotaRod test. **f**, Age-related changes in physical performance in young (3 months, $n=25$) and aged mice (20 months, $n=35$). **g**,**h**, Intra- (**g**) and intergroup (**h**) comparison of average time spent on wheel (RotaRod test) of Young ($n=5$), Aged-PBS ($n=8$), Aged-yEOS ($n=5$) and Aged-yEOS$^{IL-4-/-}$ ($n=5$) mice. The experiment (**g**,**h**) was performed once. Changes in performance in (**d**,**h**) are calculated relative to baseline (post- minus pretreatment results). Statistical significance was calculated by unpaired two-tailed Student's *t*-test (**b**,**f**,), Wilcoxon matched pairs signed-rank test (**c**,**g**) or one-way ANOVA followed by two-tailed post hoc Dunnett's multiple comparison test against the Aged-PBS group (**d**,**h**). Data are shown as individual data points with mean ± s.e.m. * $P<0.05$, ** $P<0.01$, *** $P<0.001$. NS, not significant.

(Aged-aIL6) or isotype control (Aged-ISO) over a 4-week period (Fig. 6i). The treatment regimen employed resulted in a significant reduction in plasma IL-6 levels in Aged-aIL6 mice compared to the Aged-ISO group (Fig. 6j). Importantly, blocking of systemic IL-6 responses in aged mice mimicked the phenotype of the rejuvenating effects observed in Aged-yEOS mice in physical endurance tests (Fig. 6k,l). However, compared to Aged-yEOS mice (Fig. 4e,f), intra-individual improvents in strength tests in Aged-aIL-6 mice did not show a positive difference (Fig. 6m,n), suggesting that anti-IL6 treatment does not rejuvenate, but rather halts, an age-related progressive decline in muscle strength. Thus, IL-6 may represent one of multiple factors contributing to systemic inflamm-ageing and associated age-related decline in physical fitness.

Eosinophils from young donors restore age-related myeloid skewing of the HSPC lineage. To test another compartment known to progressively lose its function with age, we investigated the impact of eosinophil-mediated reduction in systemic low-grade inflammation on bone marrow haematopoiesis of aged mice. While hematopoiesis is tightly balanced in young mice, haematopoietic stem/progenitor cells (HSPCs) are skewed towards the myeloid lineage with progression of age[36,37]. Previous studies have reported a key role of age-related pro-inflammatory mediators, such as IL-6, IL-1β and TNFα, in this reprogramming of HSPCs[38–41]. Given that transfer of eosinophils from young mice to aged recipients resulted in a reduction in local and systemic inflammation, we next investigated the composition and differentiation potential of HSPC in BM of young, aged and aged-intervention groups. In line with previous reports, the numbers of haematopoietic stem cells (LSKs) and haematopoetic stem cells (HSCs) (HSC-AD and HSC-SLAM) were elevated in aged mice compared to young controls (Fig. 7a–c)[42]. While Aged-yEOS mice showed a significant reduction in absolute numbers in HSCs compared to the Aged-PBS group, no significant changes were observed in Aged-yEOS$^{IL4-/-}$ mice (Fig. 7a–c). Along with a decrease in HSPCs in Aged-yEOS mice, absolute numbers of all HSPC sub-populations (CLPs, CMPs and GMPs) were also reduced (Extended Data Fig. 9a–c). Importantly, Aged-yNEU control mice did not show any changes in HSC and HSPC subsets and the corresponding sub-populations as compared to the Aged-PBS group (Extended Data Fig. 4e,f). To assess whether the observed changes in HSPC numbers in Aged-yEOS mice, as determined by phenotypic analysis, also translate into functional alterations, we plated BM cells from Aged-PBS, Aged-yEOS and Aged-yEOS$^{IL4-/-}$ mice in methylcellulose cultures and assessed colony formation in vitro. HSPCs from aged mice are known to generate increased proportions of monocyte colony-forming units (CFUs)[43]. Strikingly, Aged-yEOS but not Aged-yEOS$^{IL4-/-}$ mice showed significant reduction in myeloid CFUs over Aged-PBS controls (Fig. 7d), indicating that eosinophils can partially reverse age-related myeloid skewing, in part through an IL-4-dependent manner. To investigate the in vivo sustainability of eosinophil-mediated haematopoietic changes, we generated mixed BM chimeras by transferring whole BM of Young, Aged-PBS or Aged-yEOS mice (Ly5.2) together with a young congenic competitor BM (Ly5.1/2) into lethally irradiated recipient mice (Ly5.1) (Fig. 7e). Flow cytometric analysis of peripheral blood (Fig. 7f,g) revealed a decrease in myeloid output in mice receiving BM of Aged-yEOS mice as compared to Aged-PBS BM transplants (Fig. 7h). However, this effect was transient and

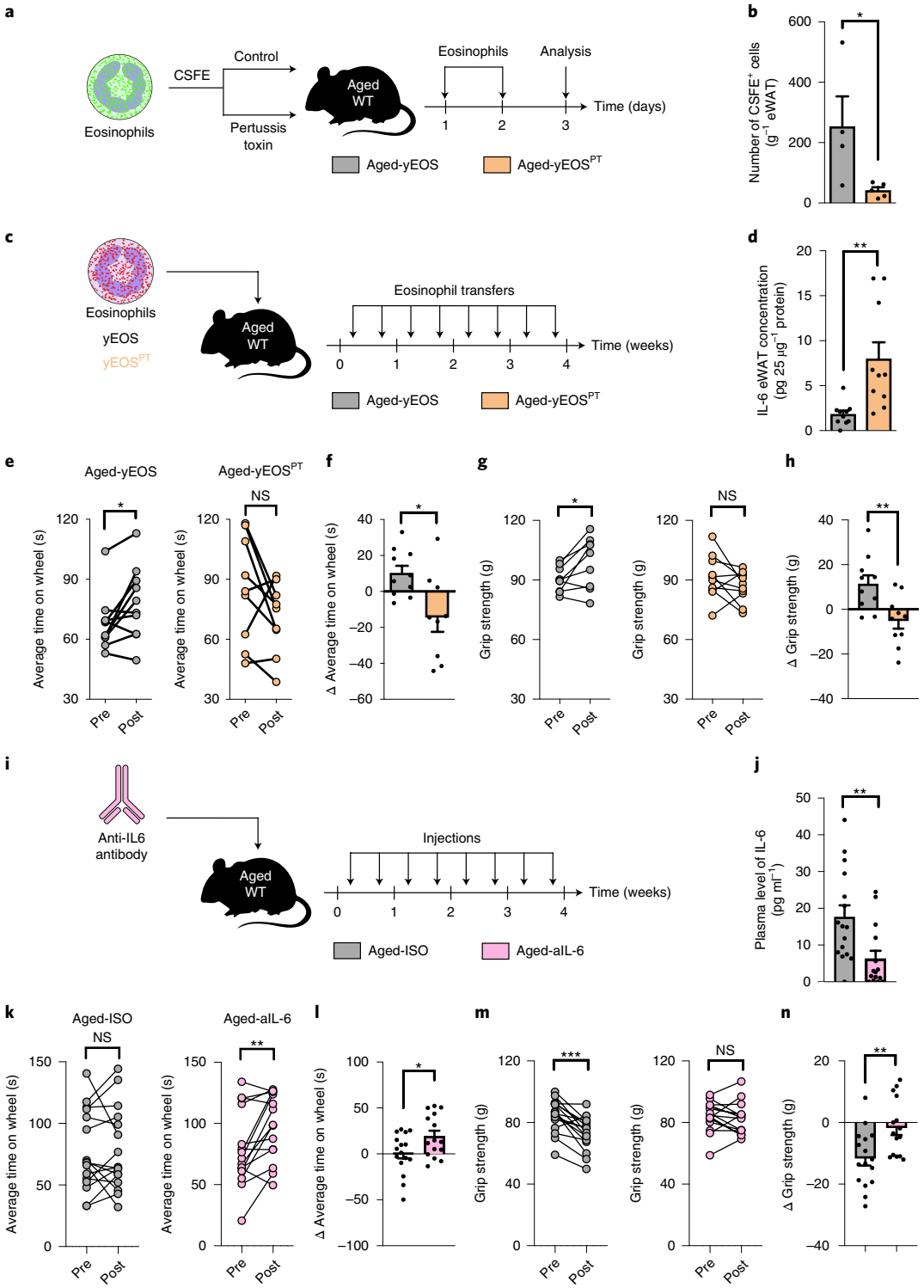

Fig. 6 | Eosinophil homing to WAT lowers age-related adipose tissue inflammation and improves physical fitness in aged recipients. a, Experimental protocol. **b**, Number of CSFE-labelled eosinophils in eWAT of control treated Aged-yEOS ($n=4$) and PT-pretreated Aged-yEOS^{PT} mice ($n=5$) as measured by flow cytometry. One of two independently performed experiments is shown. **c**, Experimental protocol. **d**, eWAT IL-6 protein levels in Aged-PBS ($n=10$) and Aged-yEOS^{PT} ($n=10$) mice. **e**,**f**, Intra- (**e**) and intergroup (**f**) comparison of average time spent on wheel (RotaRod test) of Aged-yEOS ($n=10$) and Aged-yEOS^{PT} ($n=9$) mice. **g**,**h**, Intra- (**g**) and intergroup (**h**) comparison of maximal force (grip strength, g) of Aged-yEos ($n=10$) and Aged-yEOS^{PT} ($n=10$) mice. Changes in performance for **f**,**h** were calculated relative to baseline (post- minus pretreatment results). The experiment (**c**–**h**) was performed once. **i**, Experimental protocol. **j**, IL-6 plasma levels relative to baseline (pretreatment) in Aged-ISO ($n=16$) and Aged-aIL6 ($n=15$) mice. **k**,**l**, Intra- (**k**) and intergroup (**l**) comparison of average time spent on wheel (RotaRod test) of Aged-PBS ($n=16$) and Aged-aIL6 ($n=15$) mice. **m**, Intra- and intergroup (**n**) comparison of maximal force (grip strength) of Aged-PBS ($n=16$) and Aged-aIL6 ($n=15$) mice. Changes in performance were calculated relative to baseline (post- minus pretreatment results). Data (**j**–**n**) are pooled from two independently performed experiments. Statistical significance was calculated by either Wilcoxon matched pairs signed-rank test (**e**,**g**,**k**,**m**) or unpaired two-tailed Student's *t*-test (**b**,**d**,**f**,**h**,**j**,**l**,**n**), and data are shown as individual data points with mean ± s.e.m. NS, not significant. * $P<0.05$, ** $P<0.01$, *** $P<0.001$.

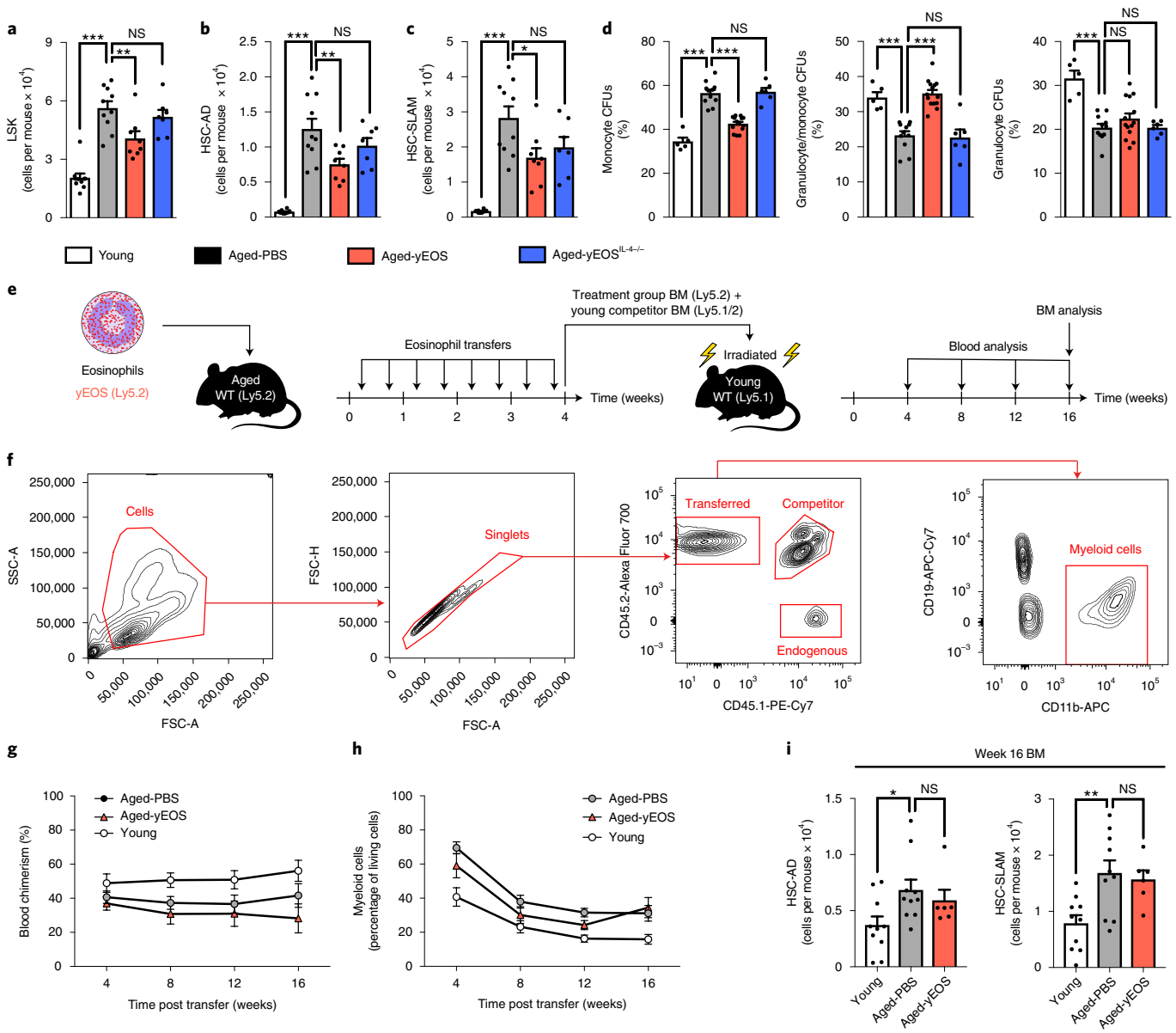

Fig. 7 | Transfer of eosinophils into aged mice transiently alters HSC numbers and age-related myeloid skewing. a, Absolute numbers of Lin$^-$, Sca-1$^+$ and c-kit$^+$ HSCs (LSKs) in Young ($n=10$), Aged-PBS ($n=10$), Aged-yEOS ($n=8$) and Aged-yEOS$^{IL\text{-}4\text{-}/\text{-}}$ ($n=7$) mice. **b**,**c**, Quantification of HSCs using CD34 and FLT3 (**b**) or SLAM markers (**c**) in indicated groups. **d**, Quantification of the percentage of monocyte colony phenotypes in plated Lin$^-$ BM methylcellulose cultures of Young ($n=5$), Aged-PBS ($n=11$), Aged-yEOS ($n=14$) and Aged-yEOS$^{IL\text{-}4\text{-}/\text{-}}$ ($n=6$) mice. Data in **a**–**d** are pooled from two independently performed experiments. **e**, Model of transplantation. **f**, Representative gating strategy to discriminate peripheral blood donor from competitor and endogenous myeloid cells. **g**, Blood chimerism of Young ($n=10$), Aged-PBS ($n=10$) and Aged-yEOS mice ($n=6$) mice. **h**, Frequencies of blood myeloid cells of Young ($n=10$), Aged-PBS ($n=10$) and Aged-yEOS mice ($n=6$) mice at indicated time points. **i**, Absolute numbers of HSC-AD and HSC-SLAM cells in Young ($n=10$), Aged-PBS ($n=10$) and Aged-yEOS mice ($n=6$) mice 16 weeks after BM transplant. **f**,**i**, The experiment was performed once. Statistical significance was calculated by one-way ANOVA followed by two-tailed post hoc Dunnett's multiple comparison test against the Aged-PBS treated group. Data are shown as individual data points with mean ± s.e.m. * $P<0.05$, ** $P<0.01$, *** $P<0.001$. NS, not significant.

disappeared over time. In line with these findings, analysis of BM revealed that mice transplanted with BM from Aged-yEOS mice had HSC numbers comparable to mice receiving Aged-PBS BM 16 weeks after transplantation. In contrast, mice transplanted with BM from young mice had significantly decreased HSC numbers compared with mice receiving BM from Aged-PBS mice (Fig. 7i). Together, our data demonstrate that eosinophils from young donors have the potential to transiently restore age-biased HSPC numbers and reverse myeloid skewing, partially mediated by eosinophil-derived IL-4.

Eosinophils from young donors boost immunological fitness in old age. Age-related changes in HSPC function contribute to poor vaccination responses and increased susceptibility to infections[44–46]. To study the functional consequences of an altered haematopoietic stem cell pool in Aged-yEOS mice, we assessed immunological fitness of aged mice in response to immunization. Young, Aged-PBS, Aged-yEOS and Aged-yEOS$^{IL4\text{-}/\text{-}}$ mice were immunized with ovalbumin (OVA) (Fig. 8a). Following secondary immunization, splenic peanut agglutinin (PNA)-positive germinal centre B cells were quantified using a flow cytometric approach (Fig. 8b

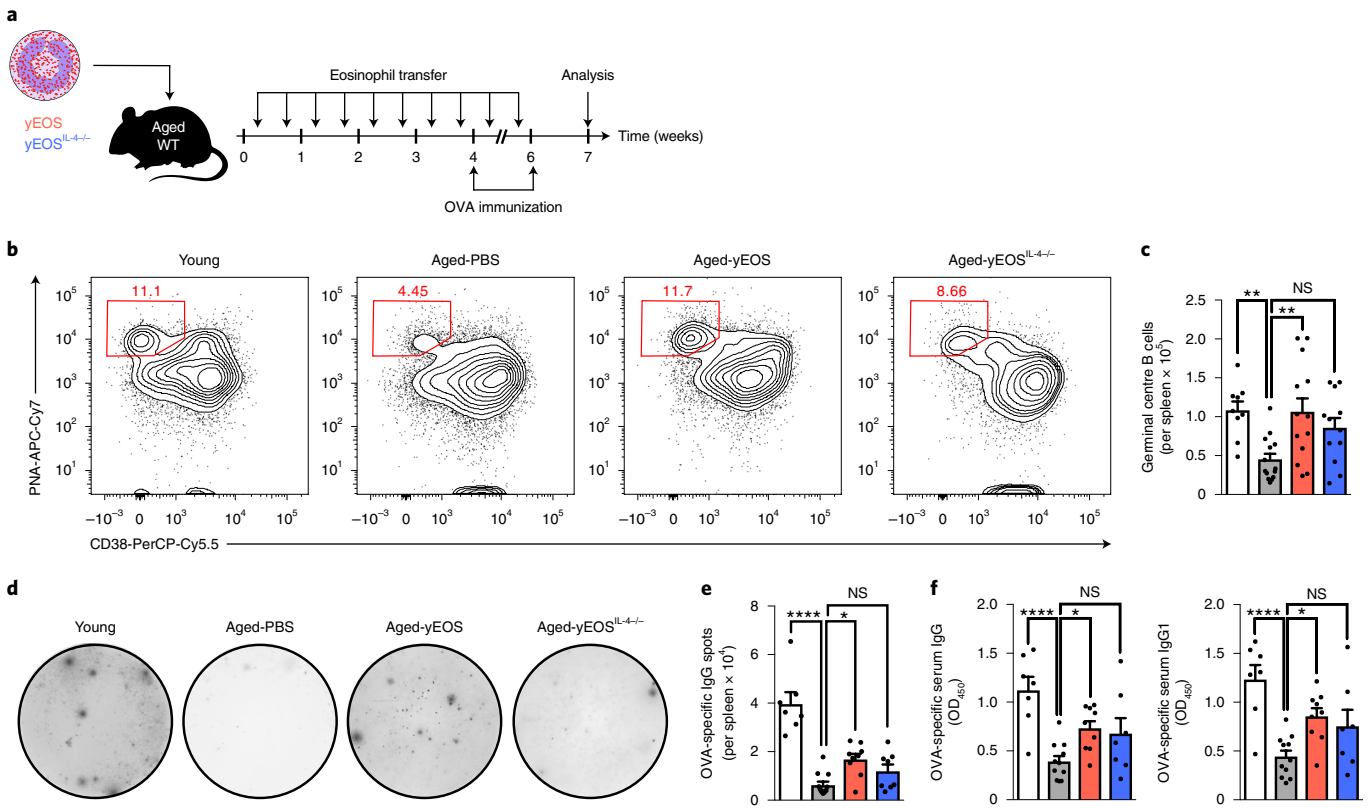

Fig. 8 | Transfer of eosinophils into aged mice is associated with improved immunological fitness. a, Immunization protocol. **b**, Representative flow plots of germinal centre B cell (PNA^+, $CD38^-$) populations in spleens of indicated groups. **c**, Total numbers of germinal centre B cells in Young ($n=9$), Aged-PBS ($n=14$), Aged-yEOS ($n=13$) and Aged-$yEOS^{IL\text{-}4\text{-}/\text{-}}$ ($n=12$) mice. **d**,**e**, Representative photographs (**d**) and quantification (**e**) of OVA-specific IgG immunospots derived from splenocyte cultures of Young ($n=7$), Aged-PBS ($n=12$), Aged-yEOS ($n=9$) and Aged-$yEOS^{IL\text{-}4\text{-}/\text{-}}$ ($n=7$) mice. **f**, Quantification of OVA-specific serum IgG and IgG1 of Young ($n=7$), Aged-PBS ($n=11$), Aged-yEOS ($n=9$) and Aged-$yEOS^{IL\text{-}4\text{-}/\text{-}}$ ($n=7$) mice. Data in **b**–**f** are pooled from two independently performed experiments. Statistical significance was calculated by one-way ANOVA followed by two-tailed post hoc Dunnett's multiple comparison test against the Aged-PBS group. Data are shown as individual data points with mean ± s.e.m. * $P<0.05$, ** $P<0.01$, *** $P<0.001$, **** $P<0.0001$. NS, not significant.

and Extended Data Fig. 9d). We found decreased numbers of splenic antigen-specific germinal centre B cells in Aged-PBS compared to Young mice after immunization. This age-related decline was restored in the Aged-yEOS and, to a lesser extent, in the Aged-$yEOS^{IL4\text{-}/\text{-}}$ group, with no intergroup significance (Fig. 8b,c). Similar results were obtained using an OVA-specific IgG ELISpot assay with splenocytes. While spleens of Aged-PBS mice harboured significantly fewer OVA-specific IgG producing B cells than their Young counterparts, transfer of IL-4-competent eosinophils into aged mice partially restored these numbers (Fig. 8d,e). Consistent with ELISpot data, total OVA-specific IgG serum titres were significantly elevated in Aged-yEOS mice as compared to Aged-PBS (Fig. 8f). These data demonstrate that the observed age-related decline in immunization responses is plastic and can be partially reversed by adoptive transfer of eosinophils from young donors. In summary, our results demonstrate that transfer of eosinophils from young donors into aged hosts partially restores the haematopoietic stem cell pool and improves age-related immune cell dysfunction and immunological fitness.

Discussion

Collectively, this study demonstrates that dysregulated eosinophil responses in WAT represent a conserved ageing phenotype in humans and mice. We find that restoration of adipose immune homeostasis by transfer of eosinophils from young mice reduces subclinical low-grade inflammation, with widespread rejuvenating consequences for the ageing host. We demonstrate that young donor eosinophils reduce WAT and systemic low-grade inflammation, restore age-related myeloid skewing, improve physical fitness and boost immune responsiveness to immunization.

The perception of WAT and its physiological role has changed considerably over the past decade. Initially identified as an inert fat depot and energy reservoir, it is now recognized as an important endocrine immune organ fulfilling important metabolic tasks[47]. Lately, WAT has gained increasing attention as a biological driver of ageing and associated functional declines[48–50]. Various studies have highlighted ageing WAT as a major source of pro-inflammatory mediators[13,51], and gene expression databases of ageing tissues confirm these findings[21]. Given that WAT is physically connected to virtually all organs, its age-related changes seem critical for the observed system-wide pathophysiology. This hypothesis is supported by many studies demonstrating that reduction of WAT mass and dysfunction by means of exercise, caloric restriction, senolytics or bariatric surgery extends health and lifespan in various organisms[2–12]. Our data highlight that restoration of WAT dysfunction by adoptive transfer of eosinophils from young donors to aged recipients improves pre-existing ageing phenotypes, including frailty and immunosenescence (Fig. 9). Given the conserved age-related decline in ATEs in humans, our findings may have broad clinical implications and thus help to identify new anti-ageing strategies specifically targeting WAT.

Inflamm-ageing describes the age-related increase in systemic low-grade chronic inflammation, which has been suggested to

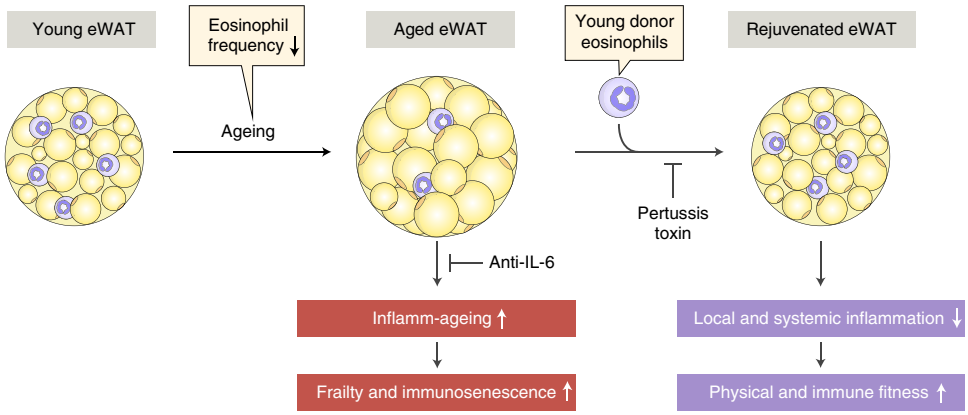

Fig. 9 | Schematic representation illustrating the rejuvenating potential of young donor eosinophils in the aged host. Age-related decrease of eosinophil frequency in eWAT is associated with the occurrence of inflamm-ageing, frailty and immunosenescence. Our study demonstrates that these ageing phenotypes are reversible following young donor eosinophil transfer, which dampens local and systemic inflammation leading to improved physical and immune fitness. The observed rejuvenation of the aged host following transfer is dependent on the migration of eosinophils into eWAT, since PT treatment of the cells abrogates these effects. Systemic blocking of IL-6 only partially mimics the phenotype of the physical improvements observed following transfer of eosinophils.

represent a common link in age-related diseases[20,52]. While there is a vast amount of literature on the direct contribution of WAT to systemic low-grade inflammation in obesity[53], direct evidence for ageing WAT as a main driver of inflamm-ageing is enigmatic and scarce. However, obesity and ageing share many aspects related to dysfunctional WAT physiology[17]. Our findings—that a reduction in inflammatory markers in WAT following eosinophil transfers (for example, IL-6, CCL2 and IL-1β) translates into reduced chronic low-grade inflammation—provides further indirect evidence that WAT may represent an important source of pro-ageing factors. To test whether bypassing the eosinophil transfer approach and directly targeting downstream inflammatory mediators that were found to be significantly changed following eosinophil transfer would result in similar rejuvenating effects, we used a protocol to deplete systemic IL-6. Importantly, previous work has demonstrated that systemic accumulation of IL-6 is not only a biomarker of ageing but also promotes age-related frailty[54,55]. Our approach, through blockage of systemic IL-6 in aged mice, confirms its pro-ageing properties in that we observed a halting or even partial reversal of age-related decline in physical performance.

Our findings highlight how transferred eosinophils efficiently migrate to WAT to restore age-related WAT dysfunction, resulting in reduced systemic low-grade inflammation and improved physical and immunological fitness. Importantly, homing of eosinophils to WAT is a prerequisite for the observed systemic rejuvenation of the aged host, as blocking of eosinophil migration to WAT by means of PT treatment failed to reproduce beneficial effects on WAT homeostasis and age-related physical deterioration. Together, these findings identify a direct link between eosinophil homing to WAT and improvements in physical fitness.

While reducing systemic low-grade inflammation by means of adoptive eosinophil transfers to aged mice resulted in improved physical performance, our findings do not support a direct effect of eosinophils on muscle function. Despite a significant increase in muscle stem cell numbers in response to eosinophil transfers, no changes in muscle mass and fibre size were observed in aged recipients. Thus, the rejuvenating potential of transferred eosinophils for physical performance of aged recipients may rather be explained by the reduction of systemic low-grade inflammation and associated improved general well-being than by a direct effect on muscle stem cells. However, these findings warrant further investigation.

Using a targeted fluidigm quantitative PCR (qPCR) array including 48 preselected eosinophil-associated genes, we further report that eosinophils in the ageing host acquire a senescent-like, pro-inflammatory phenotype (Extended Data Fig. 10 and Supplementary Table 6). This age-related eosinophil gene signature was further verified in human eosinophils (Extended Data Fig. 10c), suggesting that eosinophils might lose their migratory and regulatory function with progression of age. Consistent with the observed age-related changes in phenotype of eosinophils derived from aged donors, measures to expand endogenous eosinophils in the aged host failed to recapitulate the rejuvenating potential of transferred eosinophils from young donors (data not shown).

It has previously been reported that a sustained inflammatory milieu may promote stem cell ageing[56] and contribute to functional decline in physical and immunological performance in old age[23,43,57]. Our studies demonstrate that transfer of IL-4-competent eosinophils from young mice into aged recipients transiently restored these age-related changes in the haematopoietic stem cell pool and, consequently, improved physical and immunological fitness. Given the critical role of pro-inflammatory cytokines in multipotent haematopoietic progenitor cells and its effect on promotion of myeloid skewing[38–41], a phenomenon commonly observed in ageing, we suggest that reduction of local and systemic inflammatory mediators following transfer of young eosinophils represents an indirect mechanism to counteract these age-related haematopoietic alterations.

Because the RotaRod test represents a paradigm widely used to evaluate balance and motor coordination in the field of neuroscience, it is likely that transfer of IL-4-competent eosinophils from young mice into aged recipients may also improve age-related neuromuscular decline. Consistent with this hypothesis, IL-4 treatment has been demonstrated to improve locomotor activity and reduce axon damage in experimental models of autoimmune encephalomyelitis[58]. However, further investigations are required to determine whether eosinophil-derived IL-4 has a direct or indirect impact on stem cell reprogramming in aged organisms.

Collectively, our studies provide strong evidence that, in addition to their established role in allergic inflammation and parasitic infection, eosinophils from young organisms maintain adipose tissue homeostasis and sustain physical and immunological fitness in old age. Therapeutic targeting of WAT dysfunction in aged

individuals might therefore represent a new and promising treatment approach to promote healthy ageing.

Methods

Mouse models and drug treatment. Wild-type (WT) C57BL/6JRj young (2–3 months) and aged mice (18–22 months) were purchased either from Janvier Labs or Envigo and housed in specific pathogen-free conditions at the central animal facility of the Medical School of the University of Bern. IL-5 transgenic mice (C57BL/6J-Tg(Il5)1638Jlee, kindly provided by J. J. Lee and H.-U. Simon), C57BL/6-Il4^{tm1Nnt} and C57BL/6-Tg(UBC-GFP) 30Scha/J mice (both from The Jackson Laboratory) were bred and housed at the University of Bern and Stanford University. For transfer of IL-4-deficient eosinophils, C57BL/6J-Tg(Il5)1638Jlee mice were crossed with C57BL/6-Il4^{tm1Nnt}. For transfer of GFP^{+} eosinophils, C57BL/6J-Tg(Il5)1638Jlee mice were crossed with C57BL/6-Tg(UBC-GFP) 30Scha/J mice. InVivoMAb anti-mouse IL-6 (MP5-20F3, BioXcell) was administered through intraperitoneal (i.p.) injection twice per week. Vehicle (InVivoMAb rat IgG1 Isotype control, HRP, BioXcell) injections were performed in the same way. Treatment was initiated at 18–20 months of age for 4 weeks. Experiments were performed with age- and sex-matched control animals that were analysed side by side within each experiment. Procedures involving animal subjects were approved by the Institutional Animal Care and Use Committee, Stanford University, and the Swiss ethical guidelines were approved by the local Animal Experimentation Committee of the Canton of Bern.

Parabiosis. Parabiosis surgery was performed as previously described[18,22]. Briefly, mice were anaesthetized and the fur was shaved on adjacent flanks. Mirror-image incisions on each mouse were made through the skin. Additional incisions were made through the abdominal wall, after which the peritoneal cavities of parabionts were sutured together. Elbow and knee joints were sutured together to facilitate ease of movement, and the skin was stapled with autoclips (Clay Adams). Parabionts were given subcutaneous injections of Baytril (antibiotic) and buprenorphine (analgesia) and monitored during recovery, with 0.9% saline provided i.p. as needed for hydration. Young isochronic mice were typically 3 months of age, heterochronics 3 and 18 months of age and old isochronics 18 months of age. After 4–5 weeks of parabiosis, pairs were sedated with i.p. chloral hydrate or tribromoethanol injection and simultaneously transcardially perfused with PBS before tissue collection.

Generation of BM chimeras. Eight-week-old C57BL/6J (Ly5.1) wild-type mice were lethally irradiated by the application of 1,300 cGy in two split doses of 650 cGy with a 4-h interval, using a Gammacell 40 (GC40) research irradiator (Best Theratronics). Irradiated mice were reconstituted with 2×10^5 donor BM cells from aged mice (20 months). Whole BM cells were transplanted along with congenic competitor BM cells at a ratio of 1:1 to secure the survival of chimeric mice. Antibiotics (Baytril, 1.25 ml l^{-1} and Bactrim Nopil, 5 ml l^{-1}) were supplied in the drinking water for 2 weeks. Chimerism and white blood cell populations were analysed by flow cytometry of peripheral blood after 4, 8, 12 and 16 weeks.

Plasma collection. Healthy human blood donors were selected by specialized academic centres, based on standardized inclusion and exclusion criteria following study protocols approved by the Institute for Research in Biomedicine. Anonymized plasma samples were received, together with age and gender information. Mouse blood was collected in EDTA syringes by submandibular and/or intracardial bleeding at the time of euthanasia. Plasma was prepared by centrifugation at 1,000*g* for 10 min at 4 °C. Plasma and white blood cell fractions were recovered and prepared for subsequent flow cytometric analysis or stored at −80 °C until use.

Tissue dissection and cell preparation. Mice were euthanized with CO_2 and transcardially perfused with PBS. Muscle, liver, spleen, brain, lung, kidney, thymus, skin, mesenteric lymph node (MLN), colon, epididymal WAT (WAT) and subcutaneous fat (scWAT) were dissected, lysed, immediately snap-frozen and either formalin fixed or embedded in optimal cutting temperature compound (OCT) for further applications. Omental adipose tissue from human donors was obtained from the University Hospital of Bern, approved by the local ethics committee of the Canton of Bern under licence no. 2017-01748. All donors provided informed consent. Tissue sections were immediately fixed in 4% paraformaldehyde (PFA) overnight and embedded in paraffin for histological approaches. To separate adipocytes from the SVC fraction, visceral adipose tissue was digested in 1 mg ml^{-1} Collagenase type IV (Sigma) in RPMI medium (Gibco, supplemented with 2 nM L-glutamine, 10% FBS and 1% penicillin/streptomycin) per gram of tissue for 30 min at 37 °C on an orbital shaker, before filtration through a 70-µm cell strainer (Huber Lab). Adipocytes were separated from SVCs by centrifugation at 600*g* for 5 min. Both fractions were recovered and immediately snap-frozen on dry ice, or used for subsequent flow cytometric analyses after red blood cell lysis with ammonium-chloride-potassium (ACK) lysing buffer.

Gene expression analysis. For total RNA extraction, 100 mg of tissue was homogenized and lysed in 1 ml of TRI Reagent (Life Technologies) using a tissue lyser (Qiagen). RNA was further purified using a High Pure RNA kit (Roche) and quantified by measurement of optical density (OD) at 280-nm wavelength (NanoDrop, Thermo Scientific). Total RNA was reverse transcribed into complementary DNA using the Superscript III kit (Life Technologies). Real-time PCR was performed using SYBR Green technology (Applied Biosystems) with Qiagen QuantiTect qPCR primers for mouse *Actb*, *Tnfa*, *Il1b*, *Ccl2*, *Ccl11* and *Il6* or human *ACTB*, *TNFA*, *IL1B*, *IL6*, *P21* and *VEGFA*. All samples were run on an Applied Biosystems 7500 Real-time PCR system. Results were normalized to the housekeeping gene *Actb* and calculated as *n*-fold induction over the Aged-PBS control group, using the ΔΔCt method for all real-time PCR analyses. The fluidigm qPCR array was performed by the Stanford Human Immune Monitoring Center. Briefly, blood eosinophils from young and aged wild-type C57BL/6JRj and from young C57BL/6J-Tg(Il5)1638Jlee mice were sort purified directly into 1 ml of TRI Reagent (Life Technologies). Total RNA was purified, reverse transcribed and used for further analysis on a fluidigm qPCR array. Results from the array were normalized to the housekeeping gene *Actb* and calculated as *n*-fold induction over young using the ΔΔCt method. Values below detection threshold in young samples only were imputed with a Ct of 40 for calculation of *n*-fold induction.

Immunoblotting. Epididymal adipose tissue was prepared using M-Per lysis buffer supplemented with Halt Protease Inhibitor Cocktail (Thermo Scientific) followed by a sonication step. Total protein concentrations were determined by bicinchoninic acid (BCA; Pierce). Total protein (10–30 µg) was separated on a 12% SDS-polyacrylamide gel and transferred to a polyvinylidene difluoride membrane (BioRad). Blots were blocked with 5% skim milk followed by incubation with primary antibody overnight at 4 °C, washed (TBS-T) and incubated with secondary anti-mouse (BioRad), anti-rabbit (BioRad), anti-rat or anti-goat (both Santa Cruz) antibodies conjugated to horseradish peroxidase (HRP). Primary antibodies used were HSP-90α/β (0.5 µg ml^{-1}), CCL2 (0.1 µg ml^{-1}) and CCL11 (1 µg ml^{-1}) (R&D Systems). Antibody detection reactions were developed by chemiluminescence (Pierce) and analysed using the Las3000 imaging system (Fujifilm). Band intensities at three different locations within each band were quantified using ImageJ software[59] and normalized to HSP-90α/β. Where indicated, levels have been calculated and are expressed per total adipose tissue mass.

Enzyme-linked immunosorbent assay (ELISA). IL-1β, IL-6 and MCP-1 cytokine levels were determined in cell lysates (from adipose tissue) and plasma samples by ELISA (IL-6 and MCP-1 from BioLegend and IL-1β from Invitrogen), using the manufacturer's instructions, in 96-half-well Maxisorp plates. Cytokine binding was developed with 3,3′,5,5′-tetramethylbenzidine (TMB) and stopped with 1 M sulfuric acid. Absorbance was measured at OD_{450} nm on a standard ELISA reader from BioTek (Bad Friedrichshall). Assay sensitivities for ELISA kits are 2 pg ml^{-1} (IL-6), 30 pg ml^{-1} (MCP-1) and 1.2 pg ml^{-1} (IL-1β).

OVA-specific serum IgG ELISA was performed with a 96-half-well Maxisorp plate. Between each step, the plate was washed four times with 200 µl of PBS/0.05% Tween and twice with 200 µl of PBS. Ovalbumin (10 ng ml^{-1}) was immobilized overnight at 4 °C in 50 µl of PBS. The following day, the wells were blocked with PBS/0.5% casein for 2 h at room temperature. Subsequently, different mouse sera (diluted in PBS/0.5% casein) were added for 2 h at room temperature. Supernatants were removed and plates were washed and further incubated with either biotin goat anti-mouse IgG (1:1,000) or biotin goat anti-mouse IgG1 (1:1,000) (both BioLegend). These protein complexes were detected with poly-HRP-conjugated streptavidin (1:2,500). TMB was used as a substrate for HRP. The enzymatic reaction was stopped with 1 mol l^{-1} sulfuric acid, and absorbance was measured at a wavelength of 450 nm with an EL808 plate reader (BioTek).

Plasma from 160 human subjects between the ages of 21 and 99 years, and from 40 mice aged 6, 12, 18 and 24 months, was subjected to antibody-based multiplex immunoassay (Luminex) by either Rules Based Medicine, a fee-for-service provider, or the Human Immune Monitoring Center at Stanford University. All Luminex measurements were obtained in a blinded fashion. All assays were developed and validated to Clinical Laboratory Standards Institute (formerly NCCLS) guidelines based on the principles of immunoassay as described by the manufacturers. Detection limits for individual factors are shown in Supplementary Table 3.

Flow cytometry. Single-cell suspensions were stained with live/dead stain (Life Technologies) or propidium iodide (BD Bioscience) followed by surface and intracellular (Foxp3 transcription factor staining buffer set, Thermo Fisher) staining with fluorochrome-conjugated antibodies for subsequent flow cytometric analyses. Murine cells were stained with combinations of the following antibodies: anti-mouse CD45.2 (no. 104, BioLegend), CCR3 (no. J073E5, BioLegend), F4/80 (no. BM8, BioLegend), Siglec-F (no. E50-2440, BD Pharmingen, BD Bioscience), CD3e (nos. 145-2C11 and 17A2, BioLegend), CD19 (no. 6D5, BioLegend), CD11b (no. M1/70, BioLegend), NK1.1 (no. PK136, BioLegend), VCAM (no. 429[MVCAM.A]), integrin α7 (no. 6A11,MBL) and CD16/32 (no. 93, all BioLegend)), c-kit (no. 2B8, BioLegend), sca-1 (no. D7, BioLegend), CD127 (no. A7R34, BioLegend), CD34 (no. RAM34, BioLegend), CD51 (no. RMV-7, BioLegend), CD31 (no. 390, BioLegend), CD45 (no. 30-F11, BioLegend),

Ter-119 (no. Ter-119, BioLegend), GR1 (no. RB6-8C5, BioLegend), IgD (no. 11-26, eBioscience), B220 (no. RA3-6B2, BD Bioscience), IgM (no. II-41, BD Bioscience) and PNA-biotin, Streptavidin-PacificBlue (Molecular Probes). CountBright beads (Life Technologies) were added to each sample to determine absolute cell numbers. Eosinophils were gated as live, singlet, $CD45^+$, Lin^- (CD3, CD19, NK1.1) cells co-expressing CD11b and Siglec-F. Macrophages were gated as live, singlet, $CD45^+$, Lin^- (CD3, CD19, NK1.1) cells co-expressing CD11b and F4/80.

Human omental adipose tissue stromal vascular fraction (1×10^6 cells) was stained with live/dead stain (Life Technologies) followed by a combination of anti-human CD16 (no. 3G8, BioLegend), Biotinylated major basic protein (MBP; no. BMK-13, BioRAD), CD11b (no. ICRF44, BioLegend), Siglec-8 (no. 7C9, BioLegend), CD193 (no. 5E8, BioLegend), CD3 (no. OKT3, BioLegend), CD19 (no. HIB19, BioLegend), CD56 (no. HCD56, BioLegend) and Streptavidin-PE (eBioscience). Human adipose tissue eosinophils were gated as live, singlet, $CD45^+$, Li^- (CD3, CD19, CD56), $CD16^-$ and $CD11b^+$ cells co-expressing MBP and Siglec-8. Stained samples were supplemented with CountBright Absolute Counting Beads (Invitrogen) and acquired on a BD LSRII flow cytometer (BD Biosciences). Data were analysed using FlowJo software (FlowJo LCC).

Sort purification and adoptive transfers. Terminal bleeding of wild-type, C57BL/6J-Tg(Il5)1638Jlee and C57BL/6J-Tg(Il5)1638Jlee-UBI-GFP$^+$ mice or C57BL/6J-Tg(Il5)1638Jlee on an IL-4-deficient background (2–3 months) was performed, and red blood cells were lysed with ACK buffer. Primary eosinophils and ex vivo generated wild-type BMDEs were sort purified using a BD FACSAria III cell sorter (BD Bioscience) to ≥98% purity as live, $CD45^+$, $CD3^-$, $CD19^-$, $NK1.1^-$, $GR1^{int}$, $CD11b^+$ and Siglec-F^+ cells. Eosinophils (1.5×10^6) were immediately transferred by i.p. injection to the indicated aged recipients. Transfers were performed twice weekly for four consecutive weeks. In some studies, mice were treated with eosinophils once or twice weekly or for 5 weeks, twice weekly. As a control group, live, $CD45^+$, $CD3^-$, $CD19^-$, $NK1.1^-$, Ly6G$^+$ and $CD11b^+$ neutrophils were isolated from BM of WT C57BL/6 mice (2–3 months), and 1.5×10^6 cells was injected i.p. into aged mice twice weekly for four consecutive weeks. When indicated, eosinophils were pretreated in vitro with 100 ng ml^{-1} PT (Sigma-Aldrich) for 2 h at 37 °C in complete RPMI 1640 medium, and/or sort-purified eosinophils were labelled with CSFE (Molecular Probes) using standard protocols to distinguish endogenous from transferred eosinophils.

Isolation of muscle stem cells. Muscle stem cells (satellite cells) were isolated as described previously[60]. Briefly, hindlimb muscle tissues were collected and minced for 10 min in 50-ml Falcon tubes in 5 ml of RPMI; next, 5 ml of collagenase (Sigma; 1 mg ml^{-1}) was added with horizontal incubation on a shaker for 1 h at 37 °C at 70 r.p.m. Cells were washed with RPMI and centrifuged for 5 min at 500*g* at 4 °C. Supernatant was aspirated down to 8 ml, with the addition of 1 ml of collagenase (10 mg ml^{-1}) and 1 ml of Dispase (Roche, 10 mg ml^{-1}) in PBS. The suspension was carefully triturated 10–15 times up and down using a 20-ml pipette without clogging. Samples were incubated for 30 min on an orbital shaker. A 35-ml syringe with a 21-gauge needle was used to aspirate and eject the muscle suspension in and out of the syringe ten times. The cell suspension was washed in RPMI, and cells were transferred to a 70-µm nylon cell strainer and washed again at 500*g* for 5 min at 4 °C. Satellite cells were sort purified as $CD45^-$, $CD31^-$ and Sca-1^- cells co-expressing Vcam and integrin α7.

Histological and immunohistochemistry analysis. Omental adipose tissue from human donors, perfused mouse visceral adipose tissue and perfused hindlimb muscles were fixed in PFA overnight and embedded in paraffin. Tissue sections (8 µM) were either stained with haematoxylin and eosin (H&E) or processed for immunofluorescence staining.

Adipocyte size and numbers were assessed on H&E-stained slides. Digital images were captured at ×10 magnification using a Pannoramic caseViewer (3DHISTECH). Computerized morphometric analysis (ImageJ software) of individual adipocyte sections was performed in a blinded fashion. Approximately 500–1,000 adipocytes per sample were measured. Eosinophils in human omental adipose tissue sections were enumerated on H&E-stained slides. Digital images were analysed at ×30 magnification using the Pannoramic caseViewer (3DHISTECH). Eosinophils were defined by their nuclear morphology (nucleus with two lobes) and the presence of pink cytoplasm. Blinded and randomized 1-cm^2 sections were independently quantified by two researchers. Centrally nucleated myofibres were enumerated on randomized and blinded H&E-stained longitudinal and cross-sectional mouse muscle sections.

For cellular immunostaining, samples were first de-waxed (xylol/ethanol) followed by antigen retrieval with pepsin reagent for 20 min at 37 °C. Samples were washed three times in TBS-0.1% Triton (TBS-T) and blocked in TBS-T BSA for 1 h at room temperature in a humidified chamber. Primary antibodies were applied overnight at 4 °C in TBS-T-BSA (anti-human MBP, 1:20, BioRad; anti-mouse MBP, 1:250, provided by J. Lee; anti-mouse Perilipin, 1:200, Novus Biological). Sections were stained with secondary antibody (goat anti-mouse IgG Alexa Flour 568, goat anti-rabbit IgG Alexa Fluor 488 or goat anti-rat IgG Alexa Fluor 568, Invitrogen) for 1 h at room temperature, and mounted using Prolong Diamond Antifade Mountant with DAPI (Invitrogen) before imaging on either a three-dimensional Histech slide scanner (Pannoramic 250 Flash II, 3DHISTECH) or an Axio Imager A2 microscope (Zeiss).

Cultured muscle stem cells (formed myotubes) were fixed on day 7 in 4% PFA and stained with HSP-90 (H-114, Santa Cruz) followed by goat anti-rabbit Alexa 488 (Invitrogen) for visualization. Slides were mounted using Prolong Diamond Antifade Mountant with DAPI (Invitrogen) before imaging, and images were taken on an Axio Imager A2 (Zeiss). Both area and number of differentiated satellite cells were quantified using ImageJ. v.5. One random area from each tissue section was used for quantification.

BMDE cultures. Eosinophils were generated from BM as described previously[61]. In brief, bones of wild-type mice were flushed from the femur and tibia. Red blood cells were removed from single-cell suspension by hypotonic lysis. BM cells were cultivated in BM medium (BMMC-Medium, RPMI 1640, GIBCO) and 20% FBS, 10 U ml^{-1} penicillin, 10 µg ml^{-1} streptomycin, 2 mM glutamine, 25 mM HEPES, 1× non-essential amino acids, 1 mM sodium pyruvate and 50 µM 2-ME (all from Life Technologies). Cells were cultured with 100 ng ml^{-1} stem cell factor (SCF) and 100 ng ml^{-1} fms-like tyrosine kinase 3 ligand (FLT3L, both PeproTech) for 4 d. At day 4, the medium was exchanged and supplemented with 10 ng ml^{-1} recombinant murine IL-5 (R&D Systems). Half of the medium was replaced every other day from day 8. BMDEs were sort purified at day 14.

Myogenesis assay. A total of 1,500 muscle stem cells (satellite cells) were sort purified and plated into the wells of a Matrigel (Corning)-coated 24-well cell culture plate containing muscle stem cell growth medium (Ham's F-10 Nutrient Mix, Thermo Fisher Scientific), 20% FBS, 1× penicillin/streptomycin and 2.5 ng ml^{-1} human basic fibroblast growth factor (Sigma) as previously reported[62]. Cells were cultured at 37 °C for 7 d with growth factor added daily (2.5 ng ml^{-1}). Myotubes were stained and quantified as described in Histological and immunohistochemistry analysis.

Isolation of primary human eosinophils. Human eosinophils were isolated from volunteers, who provided informed consent in accordance with the Declaration of Helsinki. The study was approved by the local ethical committee under licence no. 108/14. Donors were defined by age (young, ≤29 years and old, ≥64 years). Briefly, peripheral human blood granulocytes were purified from venous EDTA blood by dextran sedimentation of red blood cells, followed by Percoll density gradient centrifugation (1.0791, 1.0695 and 1.9010 g ml^{-1}, GE Healthcare), and further purified by negative selection (anti-CD16 Microbeads and Glycophorine A beads, Miltenyi Biotec). Eosinophils were gated as $CD16^-$, $CD193^+$ and Siglec-8^+ cells, and absolute cell numbers and purity (≥90%) were assessed using a FACSCalibur flow cytometer (BD Biosciences) with BD Truecount Tubes (BD Biosciences).

Physical function measurements. A grip strength meter (Bioseb) was used to assess the limb strength of aged mice. To determine maximal peak force, each mouse was pulled backwards parallel to the metal bar after allowing it to be grabbed by their forelimbs. Grip strength was measured three times at 5-min intervals between triplicate measurements. Mice were adapted to the grip strength test the day before analysis. To measure forced physical activity, animals were assessed for their ability to stay on a 7-cm-diameter RotaRod (Ugo Basile). Mice were placed on the drum rotating at a constant speed of 4 r.p.m. for 20 s with constant acceleration. Animals were adapted to the RotaRod device before performing four test runs. The speed when the mouse dropped off the RotaRod was then recorded. Results were averaged from four trials and normalized, where indicated, to the baseline speed at time (*t*) zero. Data are displayed as an average of the test runs. Baseline measurements for grip strength and RotaRod were taken at t_{zero}. Differences between t_{final} (four test runs) and t_{zero} (two to three test runs) for RotaRod, and differences between t_{final} and t_{zero} (for both, an average of nine test runs) for grip strength, were calculated for each individual mouse to determine rejuvenation potential. Open field tests were used to assay general voluntary locomotor activity. In brief, mice were placed in an enclosed, rectangular box (35 × 54 cm^2) and movements within a dedicated arena were tracked for 10 min using the EthoVision system (Noldus). Movement velocity, total distance moved, accumulative mobility and immobility were recorded.

Stem cell analysis. Bone marrow lineage depletion was performed using biotinylated antibodies against red cell precursors (anti-Ter-119), B cells (anti-CD19), T cells (anti-CD3ε) and myeloid cells (anti-Gr1), and magnetic-activated cell separation (MACS) anti-biotin beads and LS columns (Miltenyi Biotec). Colony formation assays were performed as previously described[40]. Briefly, 3.3×10^3 Lin^- cells were cultured in MethoCult base medium (STEMCELL Technologies) supplemented with 15% FCS, 20% BIT (50 mg ml^{-1} BSA in Iscove's modified Dulbecco's medium, 1.44 U ml^{-1} rh-insulin (Actrapid, Novo Nordisk) and 250 ng ml^{-1} human Holo Transferrin (ProSpec), 100 µM 2-β-mercaptoethanol, 100 U ml^{-1} penicillin, 100 µg ml^{-1} streptomycin, 2 mM L-glutamine and a cytokine mix of 50 ng ml^{-1} rm-SCF, 10 ng ml^{-1} rm-IL-3, 10 ng ml^{-1} rh-IL-6 and 50 ng ml^{-1} rm-Flt3-ligand (all from ProSpec). Total colonies and colony subsets were enumerated after 7 d.

Mesenchymal stem cells were analysed by flow cytometry as previously described[40]. Briefly, bones were crushed and digested in PBS with collagenase and DNase for 1 h at 37 °C. Stromal cells were separated from the haematopoietic fraction by removal of $CD45^+Ter\text{-}119^+$ cells with MACS. Cells were stained for CD51, Sca-1 and CD31 cells. Haematopoietic cells were excluded with lineage markers CD45 and Ter-119.

Immunization. Mice were immunized with OVA emulsified in complete Freund's adjuvant (OVA-CFA) according to the manufacturer's protocol (Hooke Laboratories). In brief, anaesthetized mice were immunized subcutaneously with 100 µl of OVA-CFA at two sites on the back. Fourteen days later, mice received a secondary subcutaneous injection (100 µl) with OVA emulsified in OVA-IFA. Seven days after secondary immunization, spleens were harvested and analysed.

ELISpot. Single-cell splenocyte suspensions were prepared by squeezing dissected spleens through a 70-µm cell strainer. Red blood cells were lysed using ACK buffer and samples centrifuged. Supernatants were discarded and cells resuspended in RPMI medium. Cells were counted using a Neubauer chamber and diluted to 2.5×10^6 cells ml^{-1}. Three 1:4 serial dilutions of cells were prepared. ELISpot plates (Millipore) were coated overnight at 4 °C with 15 µg ml^{-1} OVA (Sigma) in carbonate buffer (pH 9.6). Plates were washed twice with PBS and each well blocked with 4% skim milk for 2 h at 37 °C. Subsequently plates were washed with PBS and 100 µl of serially diluted cells was added to the wells with incubation for 12 h at 37 °C with 5% CO_2. Cells were then discarded and wells washed with PBS/0.05% Tween and PBS. Goat anti-mouse IgG (no. AT-2306-2, EY Laboratories) was added at 1:1,000 dilution in blocking buffer for 9 h at room temperature. Wells were washed with PBS/0.05% Tween and PBS. Donkey anti-goat alkaline phosphatase (no. 705-055-147, Jackson Immunochemicals) was added at 1:1,000 in blocking buffer with incubation for 3 h at room temperature on a shaker. Wells were washed with PBS/0.05% Tween and PBS. Fifty microlitres of the development solution AP Conjugate Substrate Kit (no. 1706432, BioRad) was added to each well for 3 min, and the reaction was stopped with deionized water. Immunospots were quantified using an ELISpot reader (AID).

Proteomic analysis of plasma samples. Proteomic analysis was performed in Prism (GraphPad Software) and the open source software R[63]. Human and mouse plasma datasets were preprocessed as follows: factors with >85% missing values due to concentrations below the detection threshold were excluded. For the remaining factors, missing values were imputed with the lowest measurable concentration. Plasma data were standardized by $\log_2$ transformation and z-scoring[64]. Outliers, defined as subjects with more than one factor >3 s.d. away from the mean, were excluded from the dataset. To acquire maximal matching of age and gender distribution, ten male and ten female subjects were randomly selected per age group from the human dataset; in the mouse cohort, five males and five females were included per age group. The open source software Gene Cluster v.3.0 (ref. [65]) was used for unsupervised clustering of mean values from each age group. Data were visualized using the open source software Java TreeView[66]. R software was used to calculate Spearman's rank correlations between measured factors and age.

Intraperitoneal glucose tolerance test (IPGTT) and HOMA-IR. Mice were fasted overnight for approximately 16 h. A small drop of blood from the tail vein (<5 µl) was placed on the test strip of a blood glucose meter to measure the baseline glucose level ($t = 0$). Mice were intraperitoneally injected with the appropriate amount of glucose solution (sterile 20% glucose solution required 2 g of glucose per kg body mass). The blood glucose levels were measured at 15, 30, 60 and 120 min ($t = 15$, $t = 30$, $t = 60$ and $t = 120$) after glucose injection, by placing a small drop of blood on a new test strip and recording the measurements. Insulin levels were determined with an ELISA kit (Cristal Cem) according to the manufacturer's protocols. Insulin resistance (HOMA-IR) was calculated with the following formula: [fasting glucose (mmol l^{-1}) × fasting insulin (µU ml^{-1})]/22.5.

Data and statistical analysis. All data are expressed as mean ± s.e.m. unless stated otherwise. All experiments were conducted in a randomized and blinded fashion. All treatment groups were compared for statistical analysis using GraphPad Prism v.7.0 (GraphPad Software). Pearson correlation, unpaired two-tailed Student's t-tests and paired t-tests were used to estimate statistically significant differences between two groups or repeated measurements within one group, respectively. One-way analysis of variance (ANOVA) followed by two-tailed post hoc Dunnett's multiple comparison test was used for multiple comparison. Significance was set at $P < 0.05$.

Reporting Summary. Further information on research design is available in the Nature Research Reporting Summary linked to this article.

Data availability

Additional data that support the findings of this study are available from the corresponding authors upon reasonable request. Source data for Extended Data Fig. 1 are available online.

Received: 20 December 2019; Accepted: 29 May 2020;
Published online: 06 July 2020

References

1. Palmer, A. K. & Kirkland, J. L. Aging and adipose tissue: potential interventions for diabetes and regenerative medicine. *Exp. Gerontol.* **86**, 97–105 (2016).
2. Barzilai, N., Banerjee, S., Hawkins, M., Chen, W. & Rossetti, L. Caloric restriction reverses hepatic insulin resistance in aging rats by decreasing visceral fat. *J. Clin. Invest.* **101**, 1353–1361 (1998).
3. Finkel, T. The metabolic regulation of aging. *Nat. Med.* **21**, 1416–1423 (2015).
4. López-Otín, C., Galluzzi, L., Freije, J. M. P., Madeo, F. & Kroemer, G. Metabolic control of longevity. *Cell* **166**, 802–821 (2016).
5. Gabriely, I. et al. Removal of visceral fat prevents insulin resistance and glucose intolerance of aging: an adipokine-mediated process? *Diabetes* **51**, 2951–2958 (2002).
6. Muzumdar, R. et al. Visceral adipose tissue modulates mammalian longevity. *Aging Cell.* **7**, 438–440 (2008).
7. Fontana, L., Partridge, L. & Longo, V. D. Extending healthy life span—from yeast to humans. *Science* **328**, 321–326 (2010).
8. Colman, R. J. et al. Caloric restriction delays disease onset and mortality in rhesus monkeys. *Science* **325**, 201–204 (2009).
9. Mattison, J. A. et al. Caloric restriction improves health and survival of rhesus monkeys. *Nat. Commun.* **8**, 14063 (2017).
10. Weindruch, R. The retardation of aging by caloric restriction: studies in rodents and primates. *Toxicol. Pathol.* **24**, 742–745 (1996).
11. Xu, M. et al. Senolytics improve physical function and increase lifespan in old age. *Nat. Med.* **55**, 1246–1256 (2018).
12. Hahn, O. et al. A nutritional memory effect counteracts the benefits of dietary restriction in old mice. *Nat. Metab.* **1**, 1–29 (2019).
13. Lumeng, C. N. et al. Aging is associated with an increase in T cells and inflammatory macrophages in visceral adipose tissue. *J. Immunol.* **187**, 6208–6216 (2011).
14. Rosenberg, H. F., Dyer, K. D. & Foster, P. S. Eosinophils: changing perspectives in health and disease. *Nat. Rev. Immunol.* **13**, 9–22 (2013).
15. Wu, D. et al. Eosinophils sustain adipose alternatively activated macrophages associated with glucose homeostasis. *Science* **332**, 243–247 (2011).
16. Lackey, D. E. & Olefsky, J. M. Regulation of metabolism by the innate immune system. *Nat. Rev. Endocrinol.* **12**, 15–28 (2016).
17. Pérez, L. M. et al. 'Adipaging': ageing and obesity share biological hallmarks related to a dysfunctional adipose tissue. *J. Physiol.* **594**, 3187–3207 (2016).
18. Villeda, S. A. et al. The ageing systemic milieu negatively regulates neurogenesis and cognitive function. *Nature* **477**, 90–94 (2011).
19. Franceschi, C. & Campisi, J. Chronic inflammation (inflammaging) and its potential contribution to age-associated diseases. *J. Gerontol. A* **69**, S4–S9 (2014).
20. Furman, D. et al. Chronic inflammation in the etiology of disease across the life span. *Nat. Med.* **25**, 1–11 (2019).
21. Tabula Muris Consortium. et al. Single-cell transcriptomics of 20 mouse organs creates a Tabula Muris. *Nature* **562**, 367–372 (2018).
22. Villeda, S. A. et al. Young blood reverses age-related impairments in cognitive function and synaptic plasticity in mice. *Nat. Med.* **20**, 659–663 (2014).
23. Conboy, I. M. et al. Rejuvenation of aged progenitor cells by exposure to a young systemic environment. *Nature* **433**, 760–764 (2005).
24. Katsimpardi, L. et al. Vascular and neurogenic rejuvenation of the aging mouse brain by young systemic factors. *Science* **344**, 630–634 (2014).
25. Loffredo, F. S. et al. Growth differentiation factor 11 is a circulating factor that reverses age-related cardiac hypertrophy. *Cell* **153**, 828–839 (2013).
26. Baht, G. S. et al. Exposure to a youthful circulaton rejuvenates bone repair through modulation of β-catenin. *Nat. Commun.* **6**, 7131 (2015).
27. Ruckh, J. M. et al. Rejuvenation of regeneration in the aging central nervous system. *Stem Cell.* **10**, 96–103 (2012).
28. Eggel, A. & Wyss-Coray, T. A revival of parabiosis in biomedical research. *Swiss Med. Wkly.* **144**, w13914 (2014).
29. Lee, M.-W. et al. Activated type 2 innate lymphoid cells regulate beige fat biogenesis. *Cell* **160**, 74–87 (2015).
30. Qiu, Y. et al. Eosinophils and type 2 cytokine signaling in macrophages orchestrate development of functional beige fat. *Cell* **157**, 1292–1308 (2014).
31. Lee, N. A. et al. Expression of IL-5 in thymocytes/T cells leads to the development of a massive eosinophilia, extramedullary eosinophilopoiesis, and unique histopathologies. *J. Immunol.* **158**, 1332–1344 (1997).
32. Conboy, I. M., Conboy, M. J., Smythe, G. M. & Rando, T. A. Notch-mediated restoration of regenerative potential to aged muscle. *Science* **302**, 1575–1577 (2003).
33. Shefer, G., Van de Mark, D. P., Richardson, J. B. & Yablonka-Reuveni, Z. Satellite-cell pool size does matter: defining the myogenic potency of aging skeletal muscle. *Dev. Biol.* **294**, 50–66 (2006).
34. Fairfax, K. A. et al. Transcriptional profiling of eosinophil subsets in interleukin-5 transgenic mice. *J. Leukoc. Biol.* **104**, 195–204 (2018).

35. Ohnmacht, C., Pullner, A., van Rooijen, N. & Voehringer, D. Analysis of eosinophil turnover in vivo reveals their active recruitment to and prolonged survival in the peritoneal cavity. *J. Immunol.* **179**, 4766–4774 (2007).
36. Sudo, K., Ema, H., Morita, Y. & Nakauchi, H. Age-associated characteristics of murine hematopoietic stem cells. *J. Exp. Med.* **192**, 1273–1280 (2000).
37. de Haan, G. & Van Zant, G. Dynamic changes in mouse hematopoietic stem cell numbers during aging. *Blood* **93**, 3294–3301 (1999).
38. Reynaud, D. et al. IL-6 controls leukemic multipotent progenitor cell fate and contributes to chronic myelogenous leukemia development. *Cancer Cell* **20**, 661–673 (2011).
39. Riether, C., Schürch, C. M. & Ochsenbein, A. F. Regulation of hematopoietic and leukemic stem cells by the immune system. *Cell Death Differ.* **22**, 187–198 (2015).
40. Schürch, C. M., Riether, C. & Ochsenbein, A. F. Cytotoxic $CD8^+$ T cells stimulate hematopoietic progenitors by promoting cytokine release from bone marrow mesenchymal stromal cells. *Cell Stem Cell* **14**, 460–472 (2014).
41. Pioli, P. D., Casero, D., Montecino-Rodriguez, E., Morrison, S. L. & Dorshkind, K. Plasma cells are obligate effectors of enhanced myelopoiesis in aging bone marrow. *Immunity* **51**, P351–P366 (2019).
42. Akunuru, S. & Geiger, H. Aging, clonality, and rejuvenation of hematopoietic stem cells. *Trends Mol. Med.* **22**, 701–712 (2016).
43. Geiger, H., de Haan, G. & Florian, M. C. The ageing haematopoietic stem cell compartment. *Nat. Rev. Immunol.* **13**, 376–389 (2013).
44. Shaw, A. C., Joshi, S., Greenwood, H., Panda, A. & Lord, J. M. Aging of the innate immune system. *Curr. Opin. Immunol.* **22**, 507–513 (2010).
45. Goronzy, J. J. & Weyand, C. M. Understanding immunosenescence to improve responses to vaccines. *Nat. Immunol.* **14**, 428–436 (2013).
46. Salvioli, S. et al. Inflamm-aging, cytokines and aging: state of the art, new hypotheses on the role of mitochondria and new perspectives from systems biology. *Curr. Pharm. Des.* **12**, 3161–3171 (2006).
47. Zwick, R. K., Guerrero-Juarez, C. F., Horsley, V. & Plikus, M. V. Anatomical, physiological, and functional diversity of adipose tissue. *Cell Metab.* **27**, 68–83 (2018).
48. Zoico, E. et al. Brown and beige adipose tissue and aging. *Front. Endocrinol.* **10**, 368 (2019).
49. Ghosh, A. K., O'Brien, M., Mau, T., Qi, N. & Yung, R. Adipose tissue senescence and inflammation in aging is reversed by the young milieu. *J. Gerontol. A* **74**, 1709–1715 (2019).
50. Yu, P., Yuan, R., Yang, X. & Qi, Z. Adipose tissue, aging, and metabolism. *Curr. Opin. Endocr. Metab. Res.* **5**, 11–20 (2019).
51. Wu, D. et al. Aging up-regulates expression of inflammatory mediators in mouse adipose tissue. *J. Immunol.* **179**, 4829–4839 (2007).
52. Franceschi, C., Garagnani, P., Vitale, G., Capri, M. & Salvioli, S. Inflammaging and 'Garb-aging'. *Trends Endocrinol. Metab.* **28**, 199–212 (2017).
53. Kusminski, C. M., Bickel, P. E. & Scherer, P. E. Targeting adipose tissue in the treatment of obesity-associated diabetes. *Nat. Rev. Drug Discov.* **15**, 639–660 (2016).
54. Starr, M. E., Saito, M., Evers, B. M. & Saito, H. Age-associated increase in cytokine production during systemic inflammation—II: the role of IL-1β in age-dependent IL-6 upregulation in adipose tissue. *J. Gerontol. A* **70**, 1508–1515 (2015).
55. Soysal, P. et al. Inflammation and frailty in the elderly: a systematic review and meta-analysis. *Ageing Res. Rev.* **31**, 1–8 (2016).
56. Oh, J., Lee, Y. D. & Wagers, A. J. Stem cell aging: mechanisms, regulators and therapeutic opportunities. *Nat. Med.* **20**, 870–880 (2014).
57. Geiger, H. & Van Zant, G. The aging of lympho-hematopoietic stem cells. *Nat. Immunol.* **3**, 329–333 (2002).
58. Vogelaar, C. F. et al. Fast direct neuronal signaling via the IL-4 receptor as therapeutic target in neuroinflammation. *Sci. Transl. Med.* **10**, eaao2304 (2018).
59. Schneider, C. A., Rasband, W. S. & Eliceiri, K. W. NIH Image to ImageJ: 25 years of image analysis. *Nat. Methods* **9**, 671–675 (2012).
60. Liu, L., Cheung, T. H., Charville, G. W. & Rando, T. A. Isolation of skeletal muscle stem cells by fluorescence-activated cell sorting. *Nat. Protoc.* **10**, 1612–1624 (2015).
61. Dyer, K. D. et al. Functionally competent eosinophils differentiated ex vivo in high purity from normal mouse bone marrow. *J. Immunol.* **181**, 4004–4009 (2008).
62. Zhang, H. et al. NAD^+ repletion improves mitochondrial and stem cell function and enhances life span in mice. *Science* **352**, 1436–1443 (2016).
63. R Core Team. *R: A Language and Environment for Statistical Computing* (R Foundation for Statistical Computing, 2014).
64. van den Berg, R. A., Hoefsloot, H. C. J., Westerhuis, J. A., Smilde, A. K. & van der Werf, M. J. Centering, scaling, and transformations: improving the biological information content of metabolomics data. *BMC Genomics* **7**, 142 (2006).
65. de Hoon, M. J. L., Imoto, S., Nolan, J. & Miyano, S. Open source clustering software. *Bioinformatics* **20**, 1453–1454 (2004).
66. Saldanha, A. J. Java Treeview—extensible visualization of microarray data. *Bioinformatics* **20**, 3246–3248 (2004).

Acknowledgements

We thank past and present members of the Noti, Eggel and Wyss-Coray laboratories for discussions and valuable input; A.-L. Huguenin, U. Lüthi and C. Krüger for technical support; J. J. Lee and H.-U. Simon for providing IL-5 transgenic mice; M. Fux, A. Odermatt and the DBMR FACSlab for technical support with cell sorting; the staff and animal caretakers of the Central Animal Facility in Bern for their advice and support; K. Rufibach for valuable discussions; and H. Maeker and the Stanford Human Immune Monitoring Center for their help with qPCR multiplex array. J.A. is supported by grants from École Polytechnique Fédérale de Lausanne, the Swiss National Science Foundation (no. 31003A-140780), the AgingX programme of the Swiss Initiative for Systems Biology (no. 51RTP0-151019) and the NIH (no. R01AG043930). This work was funded by the National Institute on Aging (no. R01AG053382 to S.A.V. and nos. AG045034 and DP1AG053015 to T.W.-C.), the Department of Veterans Affairs (to T.W.-C.), the Glenn Center for the Biology of Aging (to T.W.-C.), a Novartis grant for Medical-Biological Research (no. 15B100 to M.N.), a FreeNovation Novartis grant (to M.N) and by grants from the Fondation Acteria (to A.E. and M.N.) and Velux Stiftung (no. 1095 to A.E.).

Author contributions

M.N. and A.E. designed the project. D.B., C.R., R.v.B., K.I.M., A.S., Z.D., N.Z., P. Gasser, P. Guntern, H.Y., J.M.C., M.B., M.H., D.G., M.S., N.M., S.A.V., M.N. and A.E. performed the experiments. F.S. and N.G.-R. provided human samples. W.H., S.L.L., P.M.V., J.A., S.A.V. and T.W.-C. provided important advice. D.B., M.N. and A.E. analysed the data and wrote the manuscript.

Competing interests

The authors declare no competing interests.

Additional information

Extended data is available for this paper at https://doi.org/10.1038/s42255-020-0228-3.

Supplementary information is available for this paper at https://doi.org/10.1038/s42255-020-0228-3.

Correspondence and requests for materials should be addressed to M.N. or A.E.

Peer review information Primary Handling Editor: Pooja Jha.

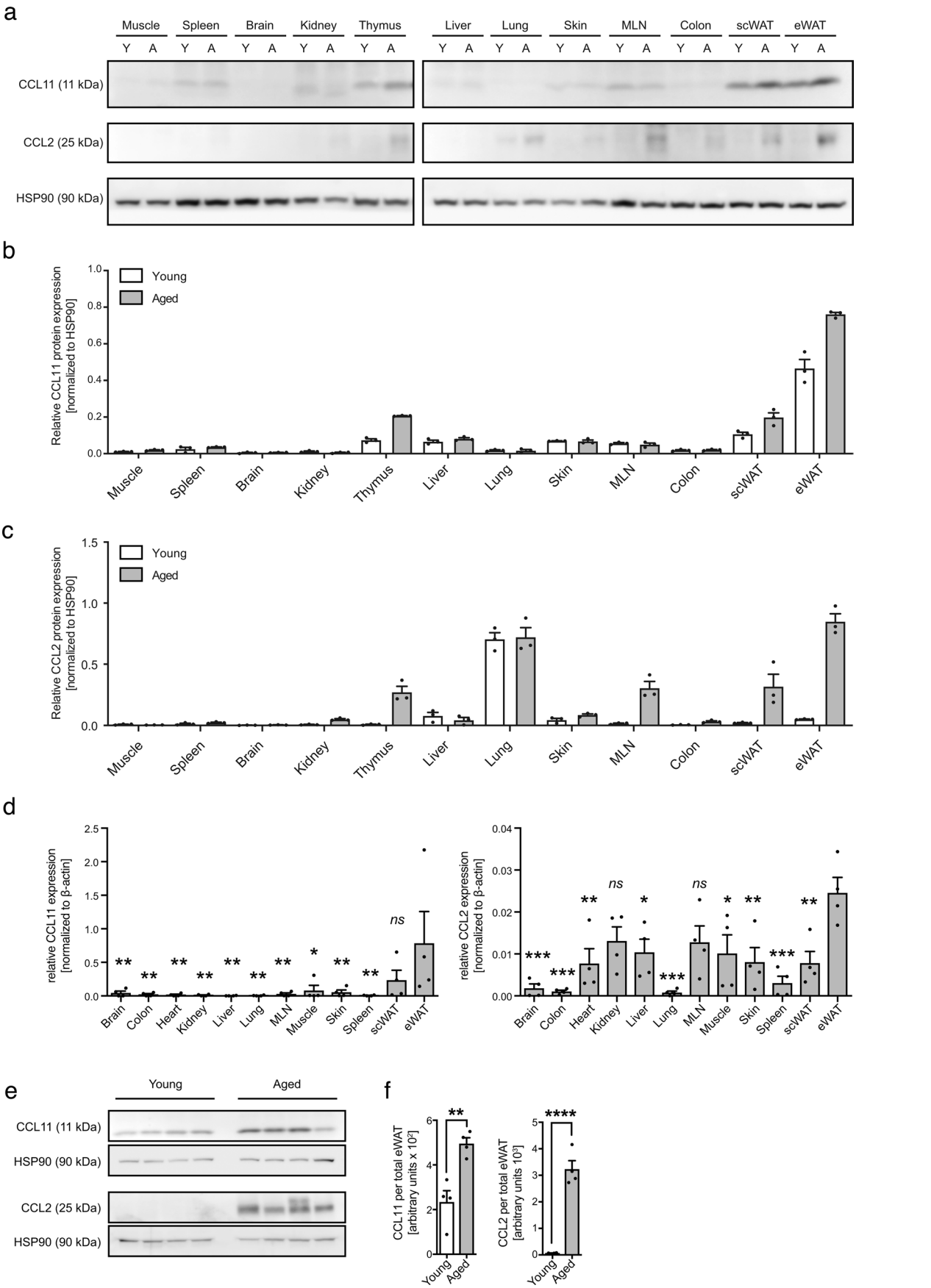

Extended Data Fig. 1 | See next page for caption.

Extended Data Fig. 1 | Tissue screens for CCL11 and CCL2 protein expression in young and aged mice. a, Comparison of CCL11 and CCL2 protein expression in muscle, spleen, brain, kidney, thymus, liver, lung, skin, mesenteric lymph nodes (MLN), colon, subcutaneous WAT (scWAT) and epididymal WAT (eWAT) of young (Y, 2-3 months) and aged mice (A, 18-20 months) as assessed by western blot. Tissues of three biologically independent animals were pooled. HSP90 served as loading control. Quantification of **b**, CCL11 and **c**, CCL2 protein levels normalized to HSP90 in indicated tissues of young (Y, 2-3 months) and aged mice (A, 18-20 months) by ImageJ. One out of two independently performed experiments is shown. **d**, Comparison of CCL11 and CCL2 mRNA expression levels in indicated tissues of aged mice (18-20 months) as assessed by qPCR (n=4). **e**, CCL2 and CCL11 protein levels were assessed by western blot (n=4). One out of 3 independently performed experiments is shown. **f**, Quantification of CCL11 and CCL2 protein levels normalized to HSP90 in indicated tissues of young (Y, 2-3 months, n=4) and aged mice (A, 18-20 months, n=4). HSP90 served as loading control. Protein levels from total eWAT was calculated. Statistical significance was calculated by one-way ANOVA followed by two-tailed post-hoc Dunnett's multiple comparison test against eWAT (**d**) or by unpaired two-tailed Student's t test between young and aged samples (**f**). Data are shown as individual data points with mean ± SEM. *p < 0.05, **p < 0.01, ***p < 0.001. *ns*, not significant. Uncropped western blots are provided in the Source Data File.

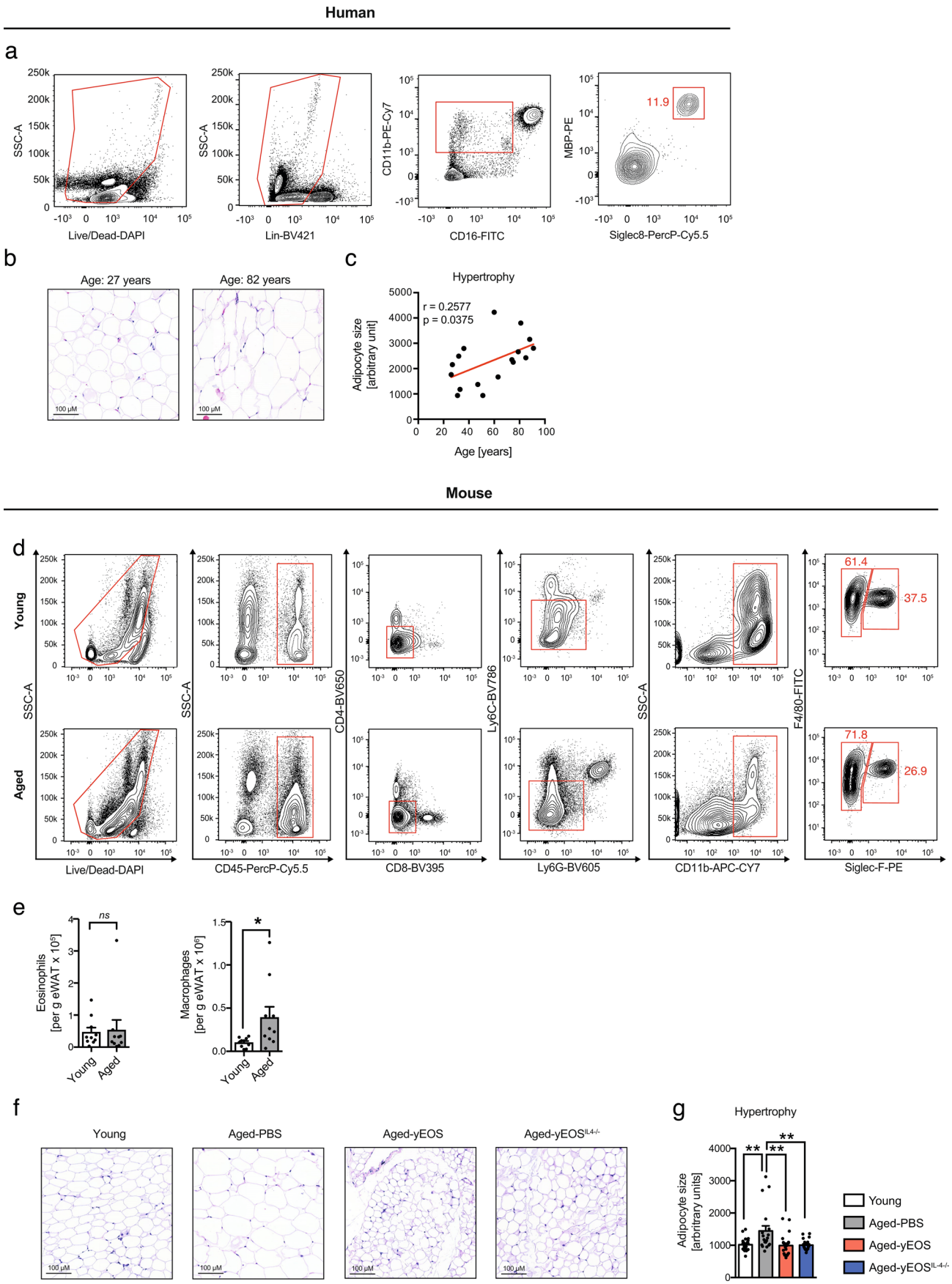

Extended Data Fig. 2 | See next page for caption.

Extended Data Fig. 2 | Gating strategies for human and mouse ATEs and age-related adipose tissue hypertrophy. a, Gating strategy for human omental adipose tissue eosinophils. **b**, Representative images of H&E stained human omental adipose tissue from young and aged donors of indicated age. Scale bar: 100 µm. **c**, Quantification of adipocyte size in H&E stained sections from human omental adipose tissue (*n*=17 biologically independent human donors) by ImageJ. **d**, Representative gating strategy for ATE (F4/80^{int}, SiglecF^{+}) and ATM (F4/80^{+}, SiglecF^{-}) in mouse visceral adipose tissue of young (3 months) and aged mice (20 months). **e**, Absolute eosinophil and macrophage numbers per gram eWAT of young (3 months, *n*=10) and aged mice (20 months, *n*=10). This experiment was done once. **f**, Representative photographs of H&E stained histological eWAT sections of indicated treatment groups. **g**, Quantification of adipocyte hypertrophy in young (*n*=20), Aged-PBS (*n*=19), Aged-yEOS (*n*=22) and Aged-yEOS$^{IL\text{-}4\text{-}/\text{-}}$ (*n*=20) biologically independent mice by ImageJ. Statistical significance was calculated by unpaired two-tailed Student's t test (**e**), the Pearson correlation coefficient between adipocyte size and age (**c**) or by one-way ANOVA followed by two-tailed post-hoc Dunnett's multiple comparison test against the aged-PBS treated group (**g**). Data are shown as individual data points with mean bars ± SEM. *$p < 0.05$, **$p < 0.01$, ***$p < 0.001$. *ns*, not significant.

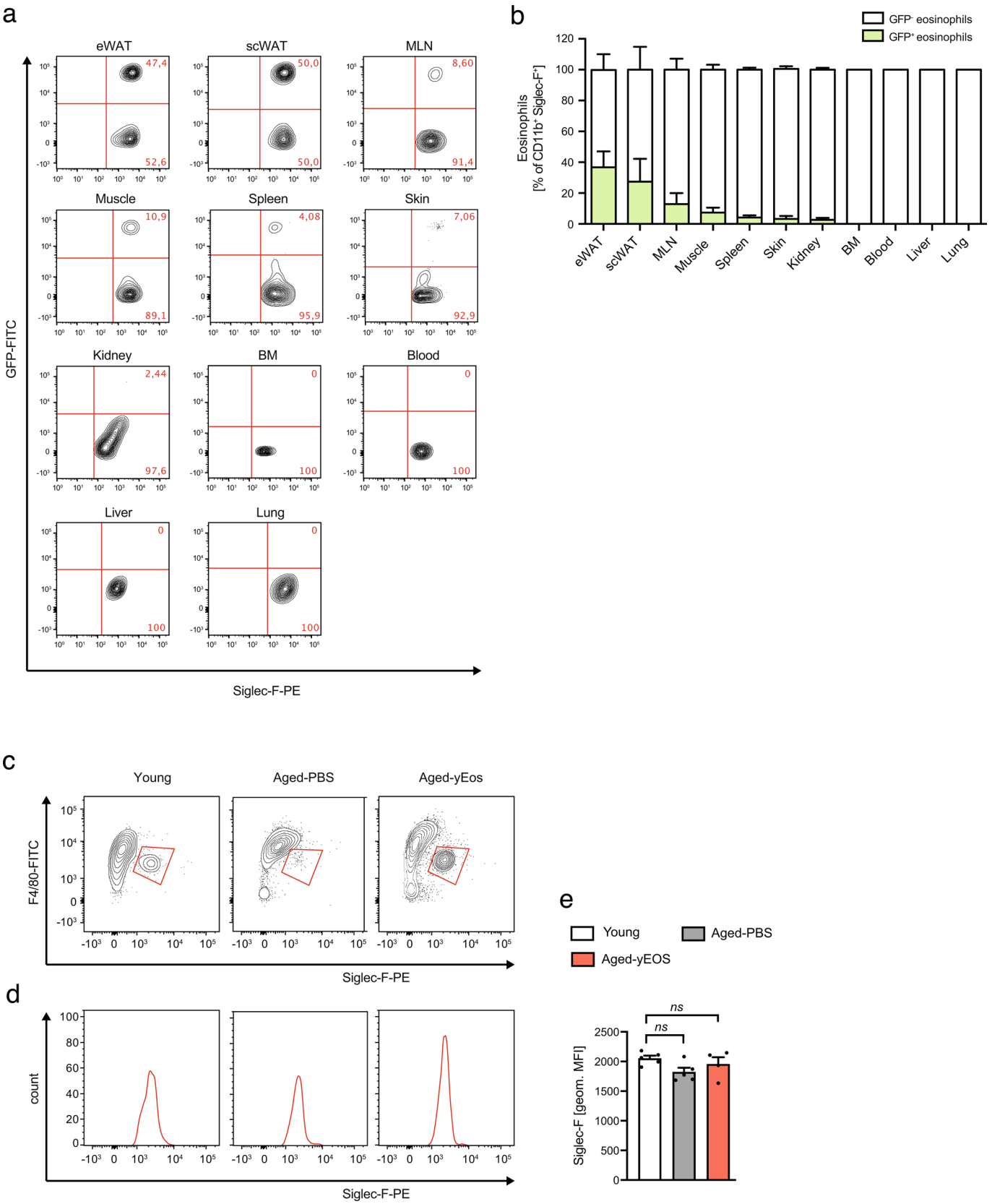

Extended Data Fig. 3 | See next page for caption.

Extended Data Fig. 3 | Recruitment of sort-purified GFP$^+$ eosinophils to WAT of aged mice. Aged mice (18 months) were adoptively transferred with sort-purified GFP$^+$ eosinophils derived from IL-5 transgenic mice on two subsequent days. The following day eosinophil recruitment into different tissues was assessed by flow cytometry. **a**, Representative flow plots of transferred GFP$^+$ and endogenous GFP$^-$ tissue eosinophils in indicated tissues. **b**, Frequencies of transferred GFP$^+$ and endogenous GFP$^-$ tissue eosinophils in indicated tissues. **c**, Siglec-F surface expression on adipose tissue eosinophils from Young, Aged-PBS and Aged-yEOS -treated mice as assessed by flow cytometry. **d**, Representative histograms of Siclec-F expression on ATEs of indicated groups. **e**, Quantification of Siglec-F surface expression (MFI) on adipose tissue eosinophils of Young (n=5), Aged-PBS (n=5) and Aged-yEOS (n=4) mice. The experiment was done once. Statistical significance was calculated by one-way ANOVA followed by two-tailed post-hoc Dunnett's multiple comparison test against the young group. *ns*, not significant. Data are representative of n=4 per group and are shown as mean ± SEM.

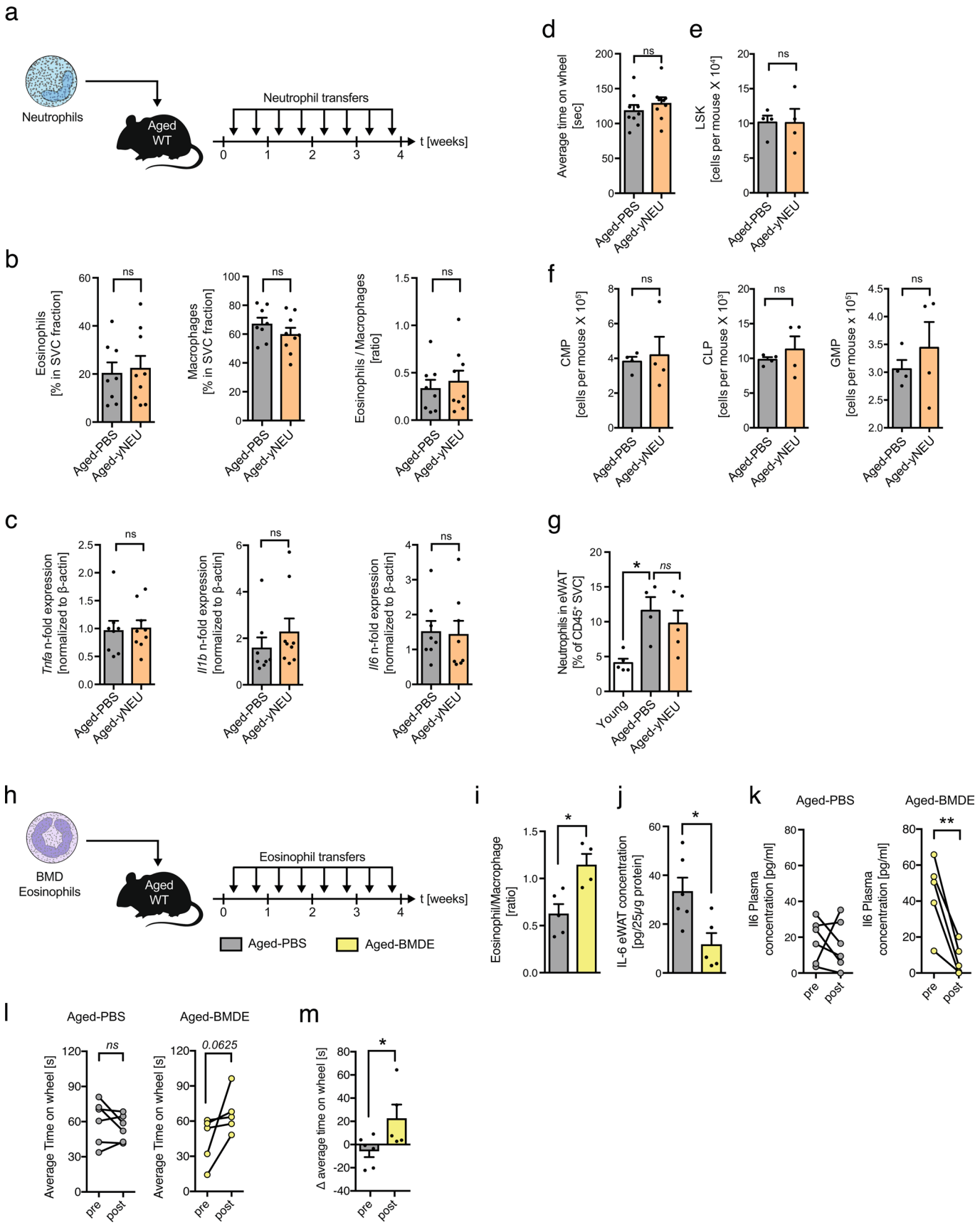

Extended Data Fig. 4 | See next page for caption.

Extended Data Fig. 4 | Transfer of neutrophils to aged mice does not alter WAT inflammation, hematopoetic stem cell pol or physical performance. **a**, Experimental protocol. **b**, Frequencies of eosinophils, macrophages and calculated eosinophil:macrophage ratios in eWAT of Aged-PBS (n=8) and Aged-yNEU (n=9) mice. **c**, mRNA expression levels for *Tnfα*, *Il1β* and *IL6* in eWAT of Aged-PBS (n=8) and Aged-yNEU mice (n=9). Data are presented as fold induction over Aged-PBS controls. **d**, Average time on Rotarod of Aged-PBS controls (n=8) and Aged-yNEU mice (n=9). **e**, Total numbers of lin$^-$, Sca-1$^+$, c-kit$^+$ hematopoietic stem cells (LSKs) in Aged-PBS (n=4) and Aged-yNEU (n=4) mice. **f**, Numbers of common myeloid progenitors (CMP), common lymphoid progenitors (CLP), and granulocyte/monocyte progenitors (GMP) in the bone marrow of Aged-PBS (n=4) and Aged-yNEU (n=4) mice. **g**, Frequencies of neutrophils in eWAT of young (n=5), Aged-PBS (n=4) and Aged-yNeu (n=5) mice. **h**, Experimental protocol of bone marrow derived eosinophil (BMDE) transfers. **i**, Calculated ATE:ATM ratios in eWAT of Aged-PBS (n=5) and Aged-BMDE (n=4) mice as measured by flow cytometry. **j**, IL-6 protein levels in eWAT of Aged-PBS (n=6) and Aged-BMDE (n=5) mice. **k**, Pre- and post-treatment IL-6 plasma protein levels in Aged-PBS (n=6) and Aged-BMDE (n=5). **l**, Intra-group and **m**, inter-group comparison of pre- and post-treatment average time on wheel (Rotarod test) in Aged-PBS (n=6) and Aged-BMDE (n=5) mice. Delta in performances in (l) is calculated relative to baseline (post- minus pre-treatment results). Statistical significance was calculated by Wilcoxon matched pairs signed rank test (**k**, **l**), by unpaired two-tailed Student's t test (**b**, **c**, **d**, **e**, **f**, **l**, **j**, **m**) or by one-way ANOVA followed by two-tailed post-hoc Dunnett's multiple comparison test against the aged-PBS treated group (**g**). Data are pooled from two independently performed experiments (except for (**g-m**) only one experiment has been performed) and shown as individual data points with mean ± SEM. Data are shown as mean ± SEM. *$p < 0.05$, **$p < 0.01$. *ns*, not significant.

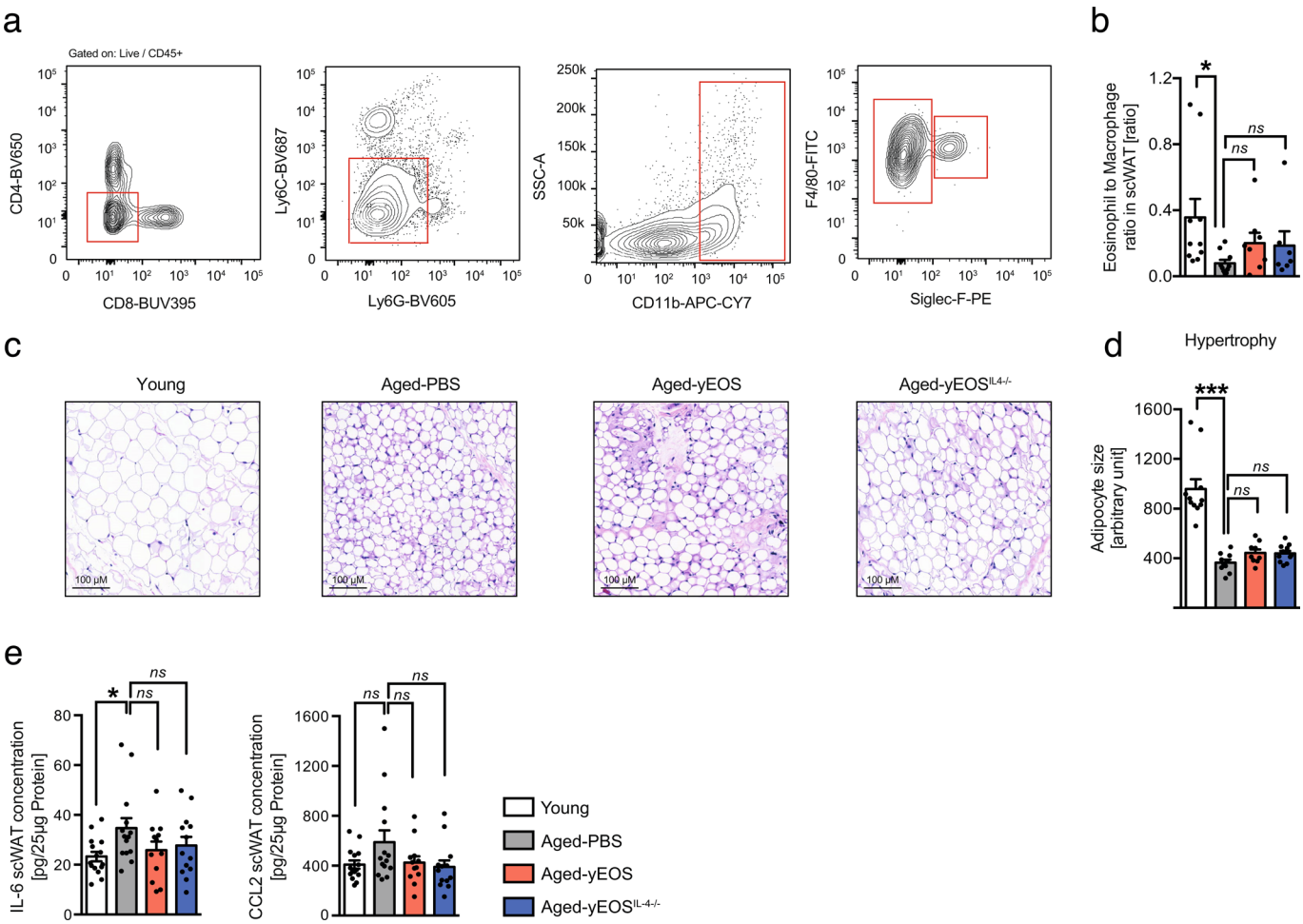

Extended Data Fig. 5 | Eosinophil transfers do not alter age-related changes in murine subcutaneous WAT. a, Gating strategy for ATMs and ATEs in scWAT of young (3 months) and aged (20 months) mice. **b**, Calculated ATE:ATM ratio in scWAT of young (n=10), Aged-PBS (n=10), Aged-yEOS (n=6) and Aged-yEOS$^{IL\text{-}4\text{-}/\text{-}}$ (n=7) mice. **c**, Representative photographs of H&E stained histological scWAT sections of indicated treatment groups. **d**, Quantification of adipocyte hypertrophy in Young (n=11), Aged-PBS (n=10), Aged-yEOS (n=9) and Aged-yEOS$^{IL\text{-}4\text{-}/\text{-}}$ (n=12) mice by ImageJ. **e**, IL-6 and CCL2 protein levels in scWAT of Young (n=15), Aged-PBS (n=14), Aged-yEOS (n=12) and Aged-yEOS$^{IL\text{-}4\text{-}/\text{-}}$ (n=13) mice. Statistical significance was calculated by one-way ANOVA followed by two-tailed post-hoc Dunnett's multiple comparison test against the aged-PBS treated group. Data (**e**) are pooled from 2 independently performed experiments or performed once (**a-d**) and shown as individual data points with mean bars ± SEM. *p < 0.05, **p < 0.01, ***p < 0.001. *ns*, not significant.

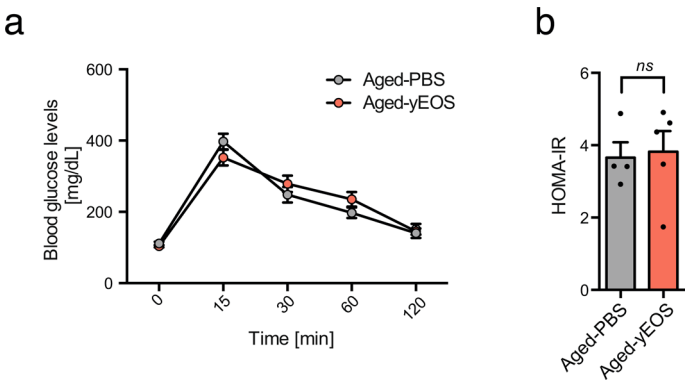

Extended Data Fig. 6 | Glucose metabolism in response to eosinophil transfers to aged mice. a, Blood glucose levels in Aged-PBS (20 months, *n*=4) and Aged-yEOS (*n*=5) mice in response to i.p. glucose challenge over time. **b**, Calculated HOMA-IR for Aged-PBS (20 months, *n*=4) and Aged-yEOS (20 months, *n*=5) mice. Statistical significance was tested by unpaired two-tailed Student's *t*-test. One out of 3 independently performed experiments is shown. Data are shown as individual data points with mean bars ± SEM. *ns*, not significant.

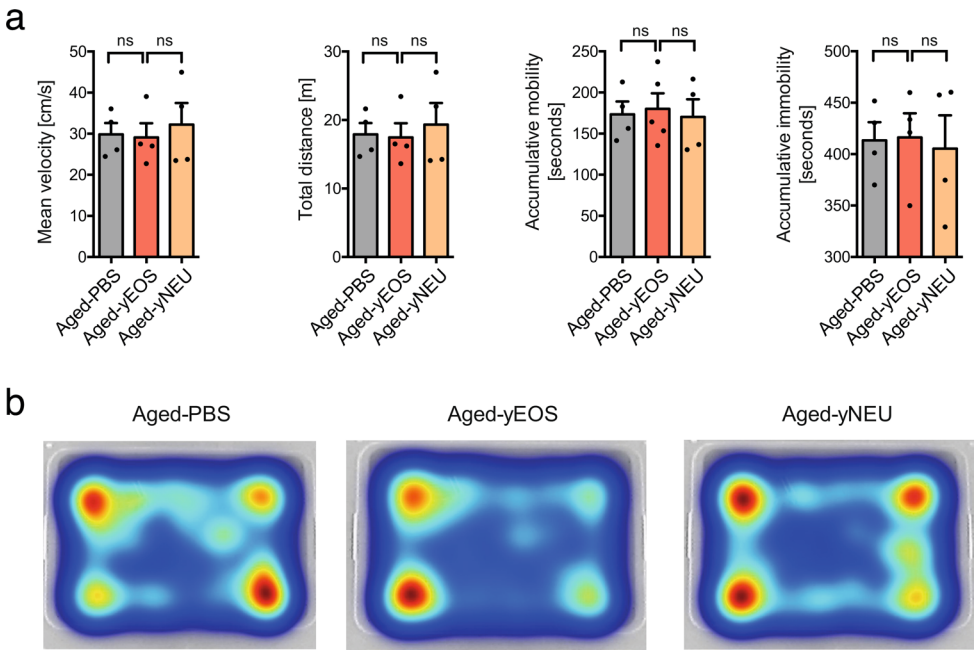

Extended Data Fig. 7 | Open field activity tests. a, Mean velocity, total distance, accumulative mobility- and immobility of Aged-PBS, Aged-yEOS and Aged-yNEU mice (n=4 per group). **b**, Representative heat maps for Aged-PBS, Aged-yEOS and Aged-yNEU mice demonstrating the animal's position in the arena. The experiment was done once. Statistical significance was calculated by one-way ANOVA followed by two-tailed post-hoc Dunnett's multiple comparison test against the aged-PBS treated group. Data are shown as mean bars ± SEM. *ns*, not significant.

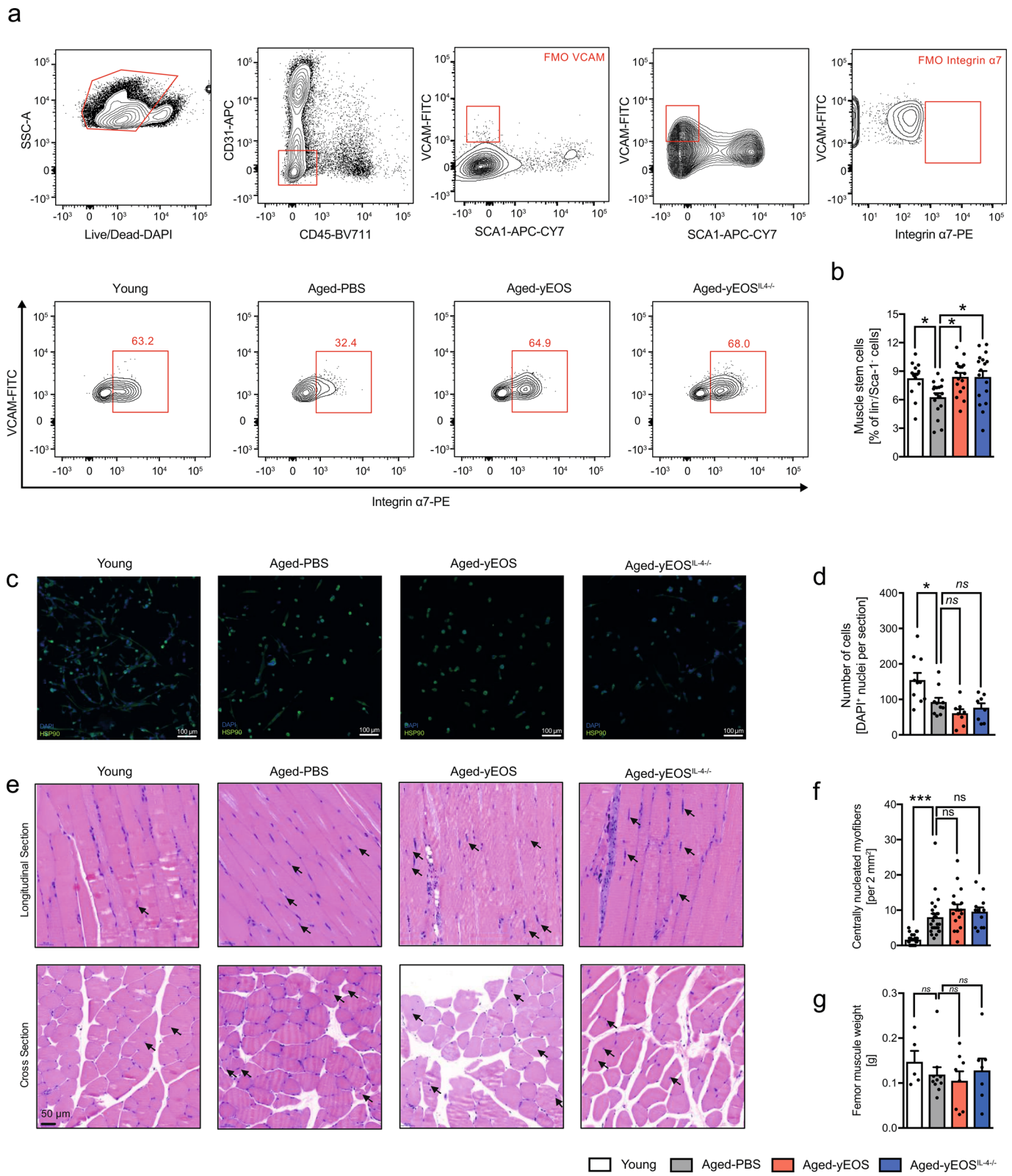

Extended Data Fig. 8 | See next page for caption.

Extended Data Fig. 8 | Transfer of young eosinophils is associated with alterations in muscle stem cell frequencies but not function. a, Gating strategy and representative flow plots of $CD31^-$, $CD45^-$, $Sca\text{-}1^-$, $Vcam^+$ and integrin $\alpha7^+$ satellite cells in muscle of Young (*n*=13), Aged-PBS (*n*=17), Aged-yEOS, (*n*=17) and Aged-yEOS$^{IL\text{-}4\text{-}/\text{-}}$ (*n*=17) mice. **b**, Quantification of muscle stem cell frequencies in indicated groups. **c**, Representative photographs of immunofluorescent stained sort-purified and differentiated satellite cells. **d**, Quantification of cell colony formation of sort-purified muscle stem cells of Young (*n*=10), Aged-PBS (*n*=10), Aged-yEOS (*n*=8) and Aged-yEOS$^{IL\text{-}4\text{-}/\text{-}}$ (*n*=8) mice **e**, Representative H&E stained longitudinal and cross-sectional quadriceps femoris in indicated groups. **f**, Quantification of centrally nucleated myofibers in sections of Young (*n*=26), Aged-PBS (*n*=26), Aged-yEOS (*n*=18) and Aged-yEOS$^{IL\text{-}4\text{-}/\text{-}}$ (*n*=13) mice. **g**, Muscle weight (femur) was measured in Young (*n*=5), Aged-PBS (*n*=9), Aged-yEOS (*n*=8) and Aged-yEOS$^{IL\text{-}4\text{-}/\text{-}}$ (*n*=7) mice. Data (**a-f**) are pooled from 2 independently performed experiments except for **g** (one experiment has been performed). Statistical significance was calculated by one-way ANOVA followed by two-tailed post-hoc Dunnett's multiple comparison test against the aged-PBS treated group. Data are shown as individual data points with mean ± SEM. *p < 0.05, **p < 0.01, ***p < 0.001. *ns*, not significant.

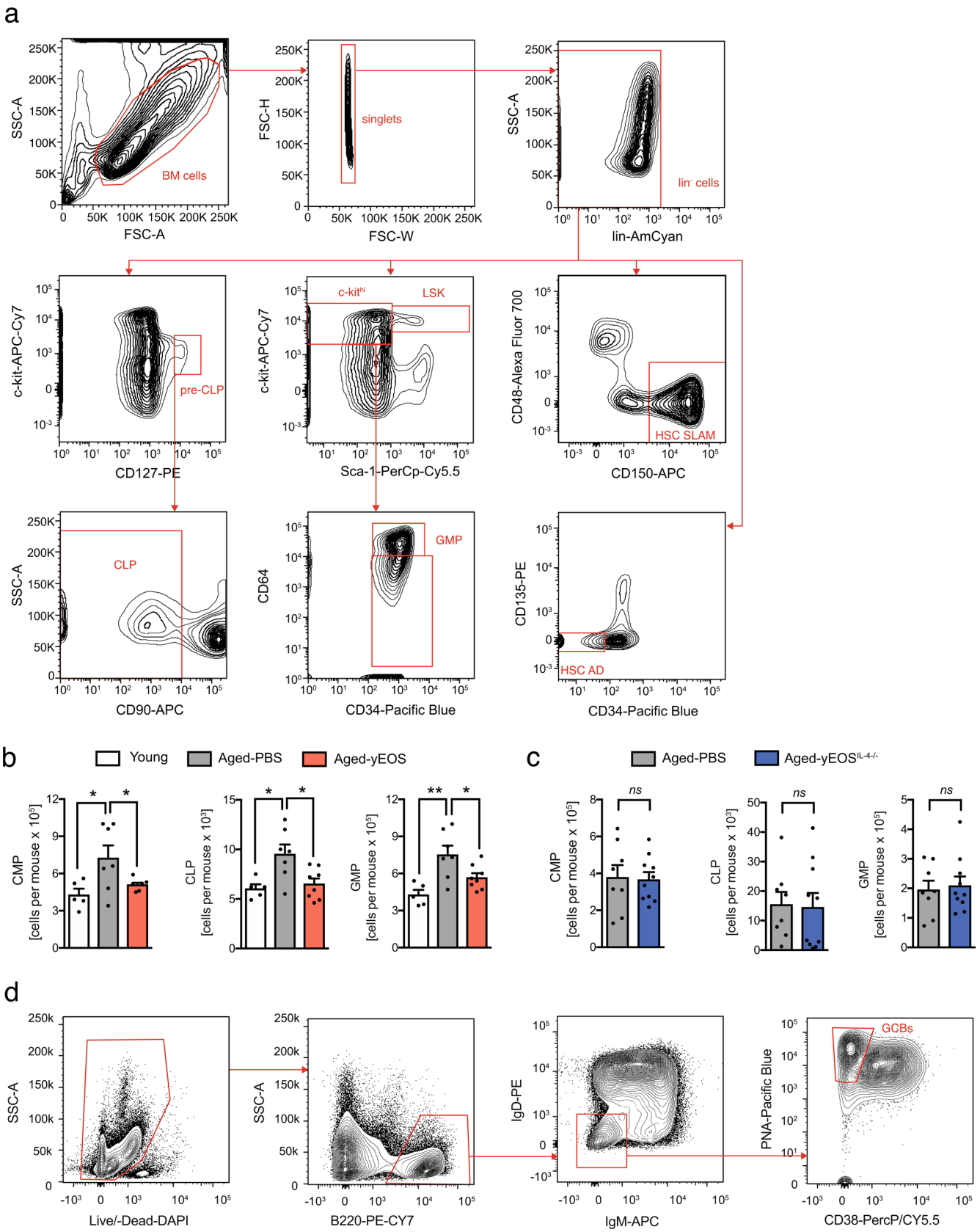

Extended Data Fig. 9 | Eosinophil transfers reverse myeloid skewing in old age. a, Gating strategy for the identification of LSK, HSC-SLAM, HSC-AD, CMP, CLP and GMP populations. **b**, Absolute numbers of CMP, CLP and GMP per mouse in Young (n=5), Aged-PBS (n=7) and Aged-yEOS (n=8) groups. **c**, Absolute numbers of CMP, CLP and GMP per mouse in Aged-PBS (n=8) and Aged-yEOS$^{IL\text{-}4\text{-}/\text{-}}$ (n=10) groups. One out of two independently performed experiments is shown. Statistical significance in (**b**) was calculated one-way ANOVA followed by two-tailed post-hoc Dunnett's multiple comparison test against the aged-PBS treated group and (**c**) by two-tailed Student's t-test. **d**, Gating strategy for the identification of germinal GCB. Data are shown as individual data points with mean ± SEM. *p < 0.05, **p < 0.01, ***p < 0.001.

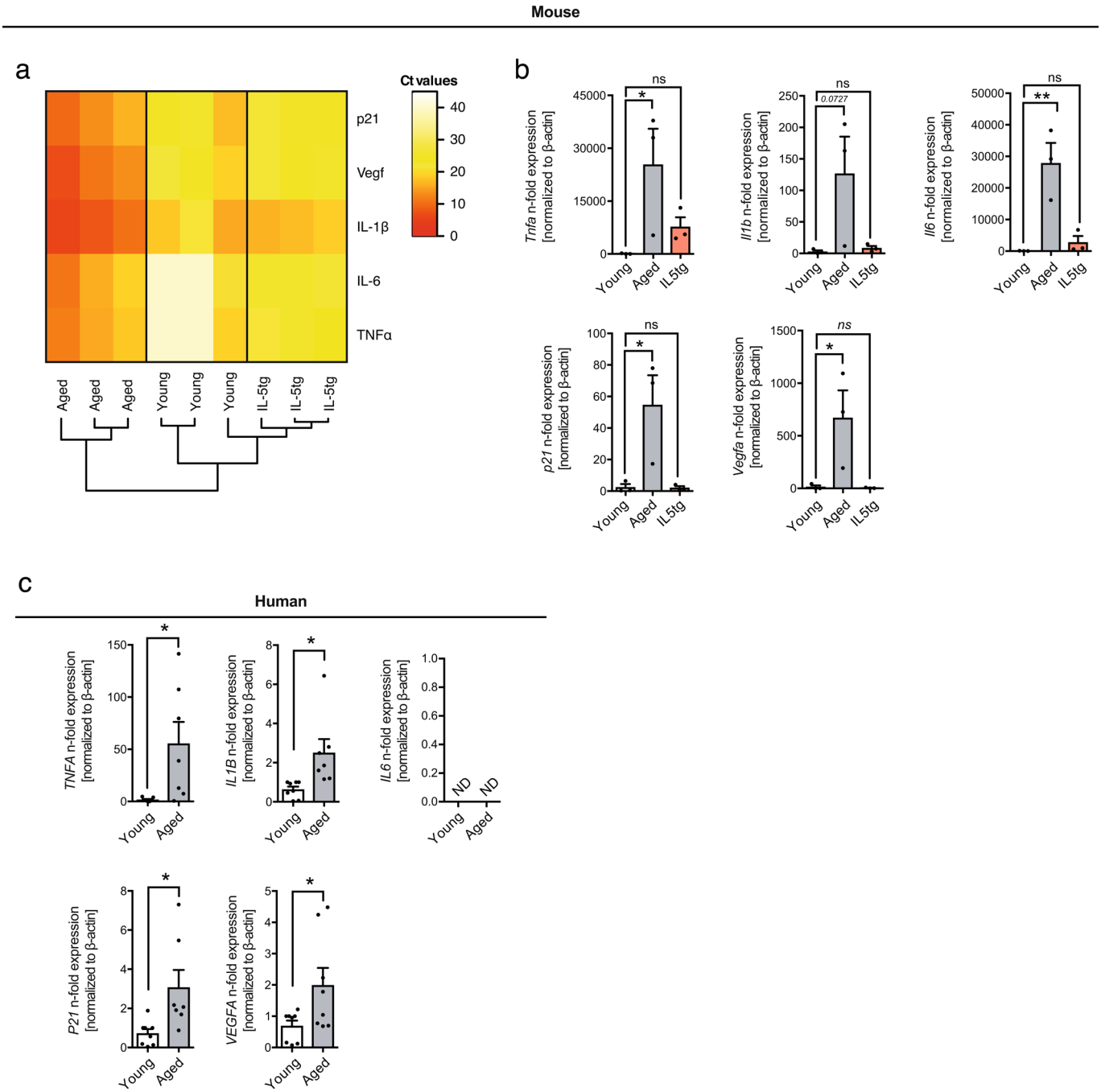

Extended Data Fig. 10 | Eosinophils adopt a senescent-like inflammatory phenotype with age. a, Heat map representing *Ct* values of *p21, Vegfa, Il1b, Il6* and *Tnfa* in sort-purified, blood-derived eosinophils from aged WT (20 months), young WT (3 months) or young IL5 transgenic mice (3 months) as assessed by targeted fluidigm qPCR array. **b**, Relative expression levels of *Tnfa, Il1b, Il6, p21* and *Vegfa* in sort-purified, blood-derived eosinophils from aged WT (20 months), young WT (3 months) or young IL5 transgenic mice (3 months) as assessed by fluidigm qPCR array. Eosinophils from 3 animals were pooled for each measurement (n=3 per group). The experiment was done once. **c**, Relative expression levels of *TNFa, IL1b, IL6, p21* and *VEGFA* in human blood derived eosinophils from young (average age=34, *n*=8) and aged (average age=64, *n*=7) donors. Data in (**b** and **c**) are shown as individual data points with mean ± SEM and statistical significance was calculated by one-way ANOVA followed by two-tailed post-hoc Dunnett's multiple comparison test against the young group (**b**) and two-tailed students *t*-test (**c**). $^{*}p < 0.05$, $^{**}p < 0.01$, $^{***}p < 0.001$. *ns*, not significant. ND, not detectable.

nature research

Corresponding author(s): Mario Noti, Alexander Eggel

Last updated by author(s): May 17, 2020

Reporting Summary

Nature Research wishes to improve the reproducibility of the work that we publish. This form provides structure for consistency and transparency in reporting. For further information on Nature Research policies, see Authors & Referees and the Editorial Policy Checklist.

Statistics

For all statistical analyses, confirm that the following items are present in the figure legend, table legend, main text, or Methods section.

n/a	Confirmed
☐	☒ The exact sample size (*n*) for each experimental group/condition, given as a discrete number and unit of measurement
☐	☒ A statement on whether measurements were taken from distinct samples or whether the same sample was measured repeatedly
☐	☒ The statistical test(s) used AND whether they are one- or two-sided *Only common tests should be described solely by name; describe more complex techniques in the Methods section.*
☐	☒ A description of all covariates tested
☐	☒ A description of any assumptions or corrections, such as tests of normality and adjustment for multiple comparisons
☐	☒ A full description of the statistical parameters including central tendency (e.g. means) or other basic estimates (e.g. regression coefficient) AND variation (e.g. standard deviation) or associated estimates of uncertainty (e.g. confidence intervals)
☐	☒ For null hypothesis testing, the test statistic (e.g. *F*, *t*, *r*) with confidence intervals, effect sizes, degrees of freedom and *P* value noted *Give P values as exact values whenever suitable.*
☒	☐ For Bayesian analysis, information on the choice of priors and Markov chain Monte Carlo settings
☒	☐ For hierarchical and complex designs, identification of the appropriate level for tests and full reporting of outcomes
☐	☒ Estimates of effect sizes (e.g. Cohen's *d*, Pearson's *r*), indicating how they were calculated

Our web collection on statistics for biologists contains articles on many of the points above.

Software and code

Policy information about availability of computer code

Data collection	Data collection was performed using Microsoft Excel (Version 14-16) and GraphPad Prism (Version 5-7).
Data analysis	Data analysis was performed in GraphPad Software Prism 7 and the open source software R (Version 2.1). The human and mouse plasma datasets were pre-processed with standard code as follows: factors with more than 85% missing values due to concentrations below the detection threshold were excluded. For the remaining factors missing values were imputed with the lowest measurable concentration. The plasma data was standardized by log2 transformation and z-scoring. Outliers defined as subjects with more than one factor that is more than 3 standard deviations away from the mean were excluded from the dataset. In order to get maximal matching of age and gender distribution 10 male and 10 female subjects were randomly selected per age group from the human dataset. In the mouse cohort 5 males and 5 females were included per age group. The open source software Gene Cluster (Version 3) was used for unsupervised clustering of mean values from each age group. Data was visualized using the open source software Java TreeView (Version 3). R software was used to calculate Spearman's rank correlations between measured factors and age. Adobe Photoshop and Illustrator (CS4-6) were used for preparation of the figures.

For manuscripts utilizing custom algorithms or software that are central to the research but not yet described in published literature, software must be made available to editors/reviewers. We strongly encourage code deposition in a community repository (e.g. GitHub). See the Nature Research guidelines for submitting code & software for further information.

Data

Policy information about availability of data

All manuscripts must include a data availability statement. This statement should provide the following information, where applicable:

- Accession codes, unique identifiers, or web links for publicly available datasets
- A list of figures that have associated raw data
- A description of any restrictions on data availability

There are no restrictions on data availability. Raw data can be provided upon request.

Field-specific reporting

Please select the one below that is the best fit for your research. If you are not sure, read the appropriate sections before making your selection.

☒ Life sciences ☐ Behavioural & social sciences ☐ Ecological, evolutionary & environmental sciences

For a reference copy of the document with all sections, see nature.com/documents/nr-reporting-summary-flat.pdf

Life sciences study design

All studies must disclose on these points even when the disclosure is negative.

Sample size	No power calculations were performed. Sample size was determined based on previous experiments and expected significance levels.
Data exclusions	Unlike otherwise stated, no data were excluded. Aged mice with obvious tumors were removed from the datasets. For plasma measurements, factors with more than 85% missing values due to concentrations below the detection threshold were excluded.
Replication	Individual experiments were repeated at least twice with similar results. Data is shown as representation of one experiment or as a combination of multiple independent experiments, as indicated in the text.
Randomization	Age- and sex-matched animals were randomly assigned to groups at the beginning of each experiment.
Blinding	The investigators were blinded for data aquisition and analysis.

Reporting for specific materials, systems and methods

We require information from authors about some types of materials, experimental systems and methods used in many studies. Here, indicate whether each material, system or method listed is relevant to your study. If you are not sure if a list item applies to your research, read the appropriate section before selecting a response.

Materials & experimental systems

n/a	Involved in the study
☐	☒ Antibodies
☒	☐ Eukaryotic cell lines
☒	☐ Palaeontology
☐	☒ Animals and other organisms
☐	☒ Human research participants
☒	☐ Clinical data

Methods

n/a	Involved in the study
☒	☐ ChIP-seq
☐	☒ Flow cytometry
☒	☐ MRI-based neuroimaging

Antibodies

Antibodies used

Antibody name, clone and provider are indicated in the materials and methods section. Antibodies were u sed as indicated by the provider.

Murine cells were stained with combinations of the following antibodies: anti-mouse CD45.2 (104, BioLegend), CCR3 (J073E5, BioLegend), F4/80 (BM8, BioLegend), Siglec-F (E50-2440, BD Pharmingen, BD Bioscience), CD3e (145-2C11 and 17A2, BioLegend), CD19 (6D5, BioLegend), CD11b (M1/70, BioLegend), NK1.1 (PK136, BioLegend), VCAM (429[MVCAM.A]), integrin □7 (6A11,MBL), CD16/32 (93, BioLegend)), c-kit (2B8, BioLegend), sca-1 (D7, BioLegend), CD127 (A7R34, BioLegend), CD34 (RAM34; BioLegend), CD51 (RMV-7, BioLegend), CD31 (390, BioLegend), CD45 (30-F11, BioLegend), Ter-119 (Ter-119, BioLegend), GR-1 (RB6-8C5, BioLegend), IgD (11-26, eBioscience), B220 (RA3-6B2, BDBioscience), IgM (II-41, BDBioscience), PNA-biotin, Streptavidin-PacificBlue (Molecular Probes). CountBrightTM beads (Life Technologies) were added to each sample to determine absolute cell numbers. Eosinophils were gated as live, singlet, CD45+, Lin- (CD3, CD19, NK1.1) cells co-expressing CD11b and Siglec-F. Macrophages were gated as live, singlet, CD45+, Lin- (CD3, CD19, NK1.1) cells co-expressing CD11b and F4/80.

Human omental adipose tissue stromal vascular fraction was stained with live/dead stain (Life Technologies) followed by a combination of anti-human CD16 (3G8, Biolegend), Biotinylated MBP (BMK-13, BioRAD), CD11b (ICRF44, Biolegend), Siglec-8 (7C9, Biolegend), CD193 (5E8, Biolegend), CD3 (OKT3, Biolegend), CD19 (HIB19, Biolegend), CD56 (HCD56, Biolegend), Streptavidin-PE (eBioscience). Human adipose tissue eosinophils were gated as live, singlet, CD45+, Lin- (CD3, CD19, CD56), CD11bInter and cells co-expressing CD193, MBP and Siglec-8.

IL-1b, IL-6, TNFa and MCP-1 cytokine levels were determined in cell lysates and plasma samples by enzyme-linked immunosorbent assay (IL-6, TNFa and MCP-1 all from Biolegend and IL-1□ from Invitrogen and Biolegend) using manufacturer`s instructions.

The InVivoMAb anti-mouse IL-6 (MP5-20F3, BioXcell) was administered through intraperitoneal (i.p.) injections twice a week.

Vehicle (InVivoMAb rat IgG1 Isotype control (HRPN, BioXcell)) injections were performed in the same way.

Western blots Blots were incubated with primary antibodies used were HSP-90a/b, CCL2 and CCL11 (R&D Systems) and secondary anti-mouse (Bio Rad), anti-rabbit (Bio Rad), anti-rat or anti-goat (both Santa Cruz) antibodies conjugated to horseradish peroxidase (HRP).

Validation

All antibodies used in this study were validated for flow cytometry, Western Blot, ELISA or ELISpot by the provider or manufacturer.

Animals and other organisms

Policy information about studies involving animals; ARRIVE guidelines recommended for reporting animal research

Laboratory animals	Wild-type (WT) C57BL/6 young (2-3 months) and aged mice (18-22months) were purchased either from Janvier Labs or Envigo and housed in specific pathogen-free (SPF) conditions at the central animal facility of the Medical School of the University of Bern. IL-5 transgenic mice C57BL/6-Tg(Il5)1638Jlee (kindly provided by Prof. James J. Lee and Prof. Hans-Uwe Simon), C57BL/6-Il4tm1Nnt and C57BL/6-Tg(UBC-GFP) 30Scha/J mice (The Jackson Laboratory) were bred at the University of Bern and Stanford University.
Wild animals	does not apply
Field-collected samples	does not apply
Ethics oversight	Procedures involving animal subjects have been approved by the Institutional Animal Care and Use Committee (IACUC) at Stanford University and the Swiss ethical guidelines approved by the local Animal Experimentation Committee of the Canton of Bern.

Note that full information on the approval of the study protocol must also be provided in the manuscript.

Human research participants

Policy information about studies involving human research participants

Population characteristics	Plasma and omental adipose tissue samples of different age groups have been collected.
Recruitment	Healthy human blood donors were selected by specialized academic centers based on standardized inclusion and exclusion criteria. Anonymized plasma samples were received together with age and gender information. Human omental adipose tissue was received from routinely intestinal resection surgery from the clinic of visceral surgery together with age, bmi and gender information.
Ethics oversight	All procedures were performed in accordance with local Institutional Review Board guidelines and have been approved by the cantonal ethics commissions (KEK/Swissethics).

Note that full information on the approval of the study protocol must also be provided in the manuscript.

Flow Cytometry

Plots

Confirm that:

☒ The axis labels state the marker and fluorochrome used (e.g. CD4-FITC).

☒ The axis scales are clearly visible. Include numbers along axes only for bottom left plot of group (a 'group' is an analysis of identical markers).

☒ All plots are contour plots with outliers or pseudocolor plots.

☒ A numerical value for number of cells or percentage (with statistics) is provided.

Methodology

Sample preparation	Tissue dissection and cell preparation: Mice were euthanized with CO2 followed by transcardial perfusion with PBS prior tissue collection. Muscle, liver, spleen, brain, lung, kidney, thymus, skin, mesenteric lymph nodes, colon, epididymal- and subcutaneous fat were dissected, lysed, immediately snap frozen, formalin fixed or embedded in OCT for further applications. Omental adipose tissue from human donors was obtained from the University Hospital of Berne and has been approved by the local ethic Committee of the Canton of Bern. All donors provided informed consent. Tissue sections were immediately fixed in 4% PFA overnight and embedded in paraffin for histological approaches. To separate adipocytes from the stromal vascular cell (SVC) fraction, visceral adipose tissue was digested in 1 mg/ml Collagenase type IV (Sigma) in RPMI medium (Gibco, supplemented with 2 nM L-glutamine, 10% FBS and 1% PenStrep) per gram tissue for 30 minutes at 37°C on an orbital shaker prior to filtration through a 70 µm cell strainer (Huber Lab). Adipocytes were separated from SVCs by centrifugation at 600g for 5 min. Both fractions were recovered and immediately snap frozen on dry ice or used for subsequent flow cytometric analyses after red blood cell lysis with ACK (Ammonium-Chloride-Potassium) lysing buffer. Isolation of primary human eosinophils. Human eosinophils were isolated from healthy volunteers who provided informed

consent in accordance with the Declaration of Helsinki. The study has been approved by the local ethic Committee under license 108/14. Donors were defined by age (young ≥ 29 and old ≤ 64). In brief: Peripheral human blood granulocytes were purified from venous EDTA-blood by dextran sedimentation of red blood cells followed by Percoll density gradient centrifugation (1.0791 and 1.0695 and 1.901 g/mL, GE Healthcare) and further purified by negative selection (anti-CD16 Microbeads and Glycophorine A beads (Miltenyi Biotec). Absolute cell number and purity was measured by FACSCalibur flow cytometer (Becton Dickinson) using BD Truecount Tubes (BD Biosciences). Eosinophil purity of higher 90% was assessed by flow cytometry as CD16-, CD193+ and Siglec-8+ cells.

Sort-purification and adoptive transfers. Terminal bleeding of wildtype, IL-5 transgenic, IL-5-UBI-GFP+ mice or IL-5 transgenic mice on an IL4 knockout background (2-3 months) was performed and red blood cells were lysed with ACK buffer. Primary eosinophils and in vitro generated wild-type BMDE were sort purified according the following gating strategy: Live, CD45+, CD3–, CD19–, NK1.1–, GR1Int, CD11b+ Siglec-F+ eosinophils were sort-purified using a BD FACSAria™ III cell sorter (BD Bioscience) to 98% purity and 1.5x106 eosinophils were immediately transferred by intraperitoneal (i.p.) injection to indicated aged recipients. Given the eosinophil half-life of a few days in vivo, transfers were performed twice a week for 4 consecutive weeks. In some studies, mice were treated with eosinophils for once, 2 times a week or for 5 weeks, twice a week. As a control group, live, CD45 +, CD3–, CD19-, NK1.1–, Ly6G+, CD11b+ neutrophils were isolated from the bone marrow of WT C57BL/6 mice (2-3 months) and 1.5x10^6 cells were injected i.p. into aged mice twice a week for 4 consecutive weeks. When indicated, eosinophils were pre-treated in vitro with 100 ng/ml pertussis toxin (Sigma-Aldrich) for 2 h at 37°C in complete RPMI 1640 Medium and/or sort-purified eosinophils were labelled with CSFE (Molecular probes) using standard protocols to distinguish endogenous from transferred eosinophils.

Muscle stem cells (satellite cells) were isolated as described (Rando et al.). Satellite cells were sort-purified as CD45-, CD31-, Sca-1-, Vcam+ and Integrin-a7+ cells.

Instrument

- BD LSRII flow cytometer (BD Biosciences)
- BD FACSAriaTM III cell sorter (BD Bioscience)
- FACSCalibur flow cytometer (Becton Dickinson,Heidelberg, Germany)

Software

- BD FACSDIVA™ Software
- FlowJo software version 10.1 (FlowJo LCC).

Cell population abundance

- Eosinophil sorts from IL-5Tg mice: 15-20% of total live, singlet cells.
- Eosinophils in adipose tissue: 15-35% of live, singlet, CD45+ CD11b+ cells depending on age.

Gating strategy

Gating strategies see Materials and Methods sections: ''Flow cytometry''&''sort-purification''

- Mouse ATE: live, singlet, CD45+, Lin- (CD3, CD19, NK1.1) cells co-expressing CD11b and Siglec-F.
- Mouse ATM: live, singlet, CD45+, Lin- (CD3, CD19, NK1.1) cells co-expressing CD11b and F4/80.
- Eosinophils from IL-5Tg mice for sorts: Live, singlet, CD45+, CD3–, CD19–, NK1.1–, GR1int, CD11b+ Siglec-F+.
- Mouse Neutrophils: live, singlet, CD45+, CD3–, CD19-, NK1.1–, Ly6G+, CD11b+ .
- Mouse muscle stem cells: live, singlets, CD45-, CD31-, Sca-1-, VCAM+, integrin-a7+.
- Mouse GCBs: live, singlets, B220+, IgD/IgM-, CD38-, PNA+
- Mouse HSC-AD: singlets, Lin-, CD34-, CD135-
- Mouse HSC-SLAM: singlets, Lin-, CD48-, CD150+
- Human ATE: live, singlet, Lin-(CD3, CD19, CD56), CD16low, CD11+, cells co-expressing Siglec-8 and MBP.

The purity of sorted cells was determined by re-sorting a fraction of the recovered cells (>98%).

☒ Tick this box to confirm that a figure exemplifying the gating strategy is provided in the Supplementary Information.